DOE/ER/13262--6

DE90 004639

A progress report

for the period January 1, 1987 to January 1, 1990

Grant DE-FG05-84ER13262

# EXCITATION OF ATOMS AND MOLECULES IN COLLISIONS WITH FAST, HIGHLY CHARGED IONS

Submitted by the

Cyclotron Institute

Texas A&M University

College Station, TX 77843

to the

Fundamental Interactions Branch

Division of Chemical Sciences

Office of Basic Energy Sciences

U.S. Department of Energy

Principal Investigator

Rand L. Watson, Professor of Chemistry

January 1, 1988

---

## TABLE OF CONTENTS

## I. INTRODUCTION

This report summarizes progress in research supported by DOE Grant DE-FG05-84ER13262 during the period January 1, 1987 to January 1, 1990. Contained herein are the titles of publications and presentations which have evolved from completed projects, and the titles of papers which have been submitted for publication. Summaries of projects completed or begun during this three year grant period constitute the main body of the report, while the appendix contains reprints of all publications resulting from this grant since the last reporting period.

A great deal of the effort during this grant period has been directed toward studies of recoil ions produced in collisions with fast, highly-ionized ions. Two aspects of this topic have been of particular interest; (a) delineation of the systematics of multiple ionization and electron capture by heavy ions, and (b) characterization of molecular dissociation processes induced by heavy ion impact.

With regard to item (a), an investigation of the projectile charge dependence of cross sections for Ar recoil-ion production in 1 MeV/amu oxygen ion collisions involving the capture or loss of 0, 1, and 2 electrons by the projectile has been carried out. Measurements of the cross sections for the production of Ne and Ar recoil ions having charges 1+ through 8+ (Ne) and 12+ (Ar) by 40 MeV $Ar^{13+}$ were performed for collisions in which the projectile charge changed by 0 through -2 units (Ne) and -4 units (Ar). In another project, preliminary data was obtained on the charge distributions of He, Ne, and Ar produced in collisions with 10 to 30 MeV/u $N^{7+}$ Ions.

Work on item (b) included two-fragment coincidence measurements of

the collision-induced dissociation of $O_2$ molecules. In these experiments, the time-of-flight of the first fragment to reach the detector and the time difference between the first and second fragment produced in binary dissociation events were recorded event-by-event, so as to preserve their correlation.

Another area of continued activity was the study of rapid electron transfer in multiply-ionized atoms. New measurements of the spectra of K$\alpha$ x-ray hypersatellites resulting from double K-vacancy production in oxygen compounds by 40 MeV Ar bombardment have revealed evidence of resonant multielectron transfer.

An investigation of the quenching of metastable states in 32 MeV Mg ions was completed. The experiments utilized the fact that the $1s2p\ ^3P$ state of He-like Mg and the $1s2\ell2p\ ^4P$ state of Li-like Mg have lifetimes comparable to the collision period in a gas to deduce total quenching cross sections.

As the electron-cyclotron-resonance (ECR) ion source neared completion, work was initiated on the design and construction of an atomic physics beamline to enable experiments with low energy, highly stripped ions. Construction of this beamline is now almost finished.

## II. PERSONNEL

| | |
|---|---|
| R. L. Watson | -Professor, Department of Chemistry and Cyclotron Institute (Principal Investigator) |
| C. Can | -Postdoctoral Research Associate (through August, 1987) |
| O. Heber | -Postdoctoral Research Associate (October, 87 to November, 89) |

| | |
|---|---|
| Gui-Ju Yu | -Postdoctoral Research Associate (through October, 87) |
| B. B. Bandong | -Postdoctoral Research Associate (since June, 88) |
| V. Horvat | -Postdoctoral Research Associate (since October, 89) |
| B. B. Bandong | -Graduate Research Assistant (through May, 88) |
| R. J. Maurer | -Graduate Research Assistant (through August, 88) |
| G. Sampoll | -Graduate Research Assistant |
| N. Matutina | -Graduate Research Assistant (since December, 89) |
| E. Moler | -Undergraduate Research Assistant (through August, 89) |
| P. A. Scott | -Undergraduate Research Assistant (through January, 89) |
| B. Hill | -Undergraduate Research Assistant (since June, 88) |
| T. Lotze | -Undergraduate Research Assistant (since June, 89) |

## III. PUBLICATIONS AND PRESENTATIONS

### A. Publications

R. L. Watson, J. Palinkas, G. J. Pedrazzini, B. Bandong and C. Can, "Polarization and Pressure Dependence of 2p-1s Transitions in He-Like and Li-Like Neon Recoil Ions", Phys. Rev. A35, 1510 (1987).

J. A. Demarest and R. L. Watson, "Beam-Foil Spectroscopy in the EUV Employing a Position Sensitive Microchannel Plate", Nucl. Instr. and Meth. B24/25, 296 (1987).

C. Can, R. J. Maurer, B. Bandong and R. L. Watson, "Investigation of the Distribution of $(n,\ell)$ States Populated by Beam-Foil Excitation of 32 MeV Oxygen Ions", Phys. Rev. A35, 3244 (1987).

R. J. Maurer, C. Can and R. L. Watson, "Ionization and Fragmentation of Some Simple Molecules in Collisions With 40 MeV $Ar^{13+}$ Ions", Nucl. Instr. and Meth. B27, 512-518 (1987).

R. L. Watson and R. J. Maurer, "Time-of-Flight Analysis of Dissociation Products from Collisions of 40 MeV $Ar^{13+}$ with Molecular Oxygen", Nucl. Instr. and Meth. A262, 99-105 (1987).

R. L. Watson, R. J. Maurer, B. B. Bandong and C. Can, "Molecular Fragmentation in Heavy Ion Collisions", in High Energy Ion-Atom Collisions; Eds. D. Berenyi and G. Hock (Springer-Verlag, 1988) pp. 382-393.

B. B. Bandong, R. L. Watson, J. Pálinkás and C. Can, "K X-ray Spectra of Highly Charged Recoil Ions Produced by Heavy-Ion Impact on Oxygen", J. Phys. B: At. Mol. Opt. Phys. 21 1325-1351 (1988).

J. A. Demarest and R. L. Watson, "Beam-Foil Study of Neon in the EUV with Foils of Carbon, Silver and Gold", Physica Scripta 38, 670-676 (1988).

G.-J. Yu, R. L. Watson, B. B. Bandong, C. Can, G. Sampoll, E. Moler and R. J. Maurer, "Collisional Quenching of $2^3P$ and $2^4P$ States in 33 MeV Two- and Three-Electron Mg Ions", Phys. Rev. A39, 1041-1048 (1989)

B. B. Bandong and R. L. Watson, "Resonant Multi-Electron Transfer in Solid Oxides Following Double K-Shell Ionization by Heavy-Ion Impact", Phys. Rev. A39, 1714-1724, (1989).

G. Sampoll, O. Heber, R. J. Maurer, P. A. Scott and R. L. Watson, "Two-Fragment Coincidence Studies of Molecular Coulomb Explosions Induced by Heavy Ion Impact", Nucl. Instr. and Meth. b40, 308-312 (1989).

B. B. Bandong and R. L. Watson, "Resonant Multi-Electron Transfer to Double K-Vacancy States in Oxygen Compounds", Nucl. Instr. and Meth. B40, 170-173 (1989).

O. Heber, G. Sampoll, R. J. Maurer, B. B. Bandong and R. L. Watson, "Cross Sections for Ar Recoil Ion Production by 1 MeV/amu $O^{q+}$ (q=2 through 8)", Nucl. Instr. and Meth. B40, 197-200 (1989).

O. Heber, G. Sampoll, B. B. Bandong, R. J. Maurer, E. Moler, R. L. Watson, I. Ben-Itzhak, J. L. Shinpaugh, J. M. Sanders, L. Hefner and P. Richard, "Charge Multipication Via Auger Decay of L-Vacancies in the Production of Highly Charged Ar Ions by Collisions with 1 MeV/amu $O^{q+}$ and $F^{q+}$", rapid communication in Phys. Rev. A39, 4898-4901 (1989).

### B. Pending Publications

O. Heber, G. Sampoll, B. B. Bandong, and R. L. Watson, "Charge Distributions of Ar Recoil-Ions Produced in One- and Two-Electron Capture Collisions by 16 MeV $O^{q+}$ Projectiles," Phys. Rev. A (in press)

Double and Single Ionization of Helium by High Velocity $N^{7+}$ Ions, O. Heber, B. B. Bandong, G. Sampoll, and R. L. Watson, Phys Rev. Lett. (submitted).

### C. Invited Presentations

Two-Fragment Coincidence Studies of Molecular Coulomb Explosions Induced by Heavy Ion Impact; Tenth Conference on the Application of Accelerators in Research and Industry, Denton, TX, November 7-9, 1988; Bull. Am. Phys. Soc. 33, 1694 (1988).

Progress Report: Excitation of Atoms and Molecules in Collisions with Fast, Highly-Charged Ions; IXth DOE Atomic Physics Program Workshop, Bethesda, MD, August 31-September 1, 1988.

Dissociation and Fragmentation of Molecular Gases by Fast Heavy ion impact; 3rd Chemical Congress of North America & 195th ACS National Meeting, Toronto, Canada, June 5-10, 1988.

Molecular Fragmentation in Heavy Ion Collisions, 3rd Workshop on High-Energy Ion-Atom Collision Processes, Institute of Nuclear Research, Debrecen, Hungary, August 3-5, 1987.

Ionization of Molecular Targets by Heavy Ion Impact, Institut Fur Experimentalphysik, Johannes-Kepler Universitat, Linz, Austria (July 31, 1987).

Time-of-Flight Analysis of Dissociation Products from Collisions of 40 MeV $Ar^{13+}$ with Molecular Oxygen; US/Japan Seminar on the Physics of Highly Charged Atoms produced in Heavy Ion Collisions, Kobe, Japan, March 16-20, 1987.

### D. Contributed Presentations

Multiple Ionization of He, Ne, and Ar by 10-30 MeV/u $N^{7+}$ Ions, O. Heber, B. B. Bandong, G. Sampoll, E. Moler, and R. L. Watson, Sixteenth International Conference on the Physics of Electronic and Atomic Collisions, New York, New York, July 26-August 1, 1989.

Multiple-Ionization of Gas Molecules in 40 MeV $Ar^{13+}$ Collisions, G. Sampoll, R. J. Maurer, O. Heber, P. Scott, and R. L. Watson, Tenth Conference on the Application of Accelerators in Research and Industry, Denton, TX, November 7-9, 1988; Bull. Am. Phys. Soc. 33, 1775 (1988).

Alignment of the $KL^1$ States of Al Metal and $Al_2O_3$ by Helium Ion Impact, P. A. Scott, B. B. Bandong, and R. L. Watson, Tenth Conference on the Application of Accelerators in Research and Industry, Denton, TX, November 7-9, 1988; Bull. Am. Phys. Soc. 33, 1776 (1988).

Charge State Distributions Produced in Atomic and Molecular Targets by 40 MeV $Ar^{13+}$ Ion Impact, R. J. Maurer, B. B. Bandong, C. Can, and R. L. Watson, X-Ray Spectroscopy in Atomic and Solid State Physics, (NATO, Series B: Physis Vol. 187, Eds., J. G. Ferreira and M. T. Ramos, 1987), Proceedings of NATO Advanced Study Institute, Vimeiro, Portugal, August 30-September 12, 1987.

R. J. Maurer, B. B. Bandong, C. Can and R. L. Watson, "Charge State Distributions for Neon and Oxygen Recoil Ion Production by 40 MeV Argon Deduced form Time-of-Flight and K X-ray Measurements", XV International Conference on the Physics of Electronic and Atomic Collisions, July 22-29, 1987, Brighton, England.

### D. PhD. Dissertations

Bryan Banadian Bandong, "X-ray Decay of Multiple-Vacancy States Produced in Various Oxygen Compounds by Energetic, Heavy-Ion Collisions," Texas A&M University, May, 1988.

Richard Jay Maurer, "Ionization and Fragmentation of Molecular Gases in Collisions with MeV/amu Heavy Ions," Texas A&M University, May, 1988.

## IV. PROJECT SUMMARIES

### A. Charge State Distributions for Ar Recoil-Ions Produced in One- and Two-Electron Capture Collisions by $O^{q+}$ Projectiles

(O. Heber, G. Sampoll, B. B. Bandong, and R. L. Watson)

When a fast projectile ion captures one or more electrons in a collision with a target atom, additional electrons may be removed from the target via direct ionization, Auger cascades, and shakeoff.[1-3] In capture collisions, the charge state distribution of the (target) recoil-ions closely resembles a bell-shaped binomial distribution. Within the framework of the Independent Electron Approximation (IEA), several models have been applied to the analysis of data from recent measurements of Ar recoil-ion production under the assumption that electrons are captured from the Ar L-shell and ionized from the M-shell.[2] The Classical Trajectory Monte Carlo (CTMC) method gives the correct order of magnitude for the capture cross sections, but does a very poor job of predicting the shape of the recoil-ion charge state distribution.[2] A semiclassical approximation employing the Vlasov equation works quite well for the prediction of ionization cross sections for a Ne target, but very poorly for the prediction of capture cross sections.[5]

A recent study[7] of Ar recoil-ion production by O and F projectiles has provided evidence which indicates that in pure ionization (i.e. direct ionization unaccompanied by capture), a large and sometimes dominant contribution to the cross sections for high recoil-ion charge states is from direct ionization of the M- and L-shells followed by

Auger decay of the L-vacancies. In the present work, the consequences of the Auger decay of L-vacancies produced in electron capture collisions is investigated.

The following quantities are defined for use in formulating the model analysis:

$p_{MI}(b)$ = probability of ionizing one electron from the target M-shell

$p_{LI}(b)$ = probability of ionizing one electron from the target L-shell

$p_{LC}(b)$ = probability of capturing one electron from the target L-shell

b = impact parameter.

In terms of the above probabilities, the probability of removing j out of J electrons from the target L-shell may be written

$$P_{Lj}(b) = \binom{J}{j}[p_{LC}(b) + p_{LI}(b)]^{j}[1 - p_{LC}(b) - p_{LI}(b)]^{J-j} \quad . \qquad (1)$$

According to the binomial theorem, the term $[p_{LC}(b) + p_{LI}(b)]^{j}$ can be expressed as

$$[p_{LC}(b) + p_{LI}(b)]^{j} = \sum_{k=0}^{j} \binom{j}{k} p_{LC}^{k}(b) p_{LI}^{j-k}(b) \quad . \qquad (2)$$

Inserting Eq. (2) into Eq. (1) gives

$$P_{Lj}(b) = \binom{J}{j} \sum_{k=0}^{j} \binom{j}{k} p_{LC}^{k}(b) p_{LI}^{j-k}(b)[1 - p_{LC}(b) - p_{LI}(b)]^{J-j} \quad . \qquad (3)$$

The probability of capturing an electron from the target M-shell by projectiles with velocity >> 1 a.u. is assumed to be negligible.[2] A check of this assumption using the CTMC method yielded a value of less

than 0.01 for the ratio of the M-capture to L-capture probabilities at 1 MeV/amu. Therefore, the probability of removing n out of N electrons from the M-shell is given by

$$P_{Mn}(b) = \binom{N}{n}[p_{MI}(b)]^n[1 - p_{MI}(b)]^{N-n} . \quad (4)$$

The cross section for removing n electrons from the M-shell and j electrons from the L-shell may then be written as

$$\sigma(n,j) = 2\pi \int_0^\infty P_{Mn}(b)P_{Lj}(b)bdb . \quad (5)$$

If $P_{Mn}(b)$ is nearly constant over the range of impact parameters for which $P_{Lj}(b) > 0$, Eq. (5) may be approximated by[4]

$$\sigma(n,j) = 2\pi P_{Mn}(0) \int_0^\infty P_{Lj}(b)bdb . \quad (6)$$

The final result is obtained by substituting Eq. (3) into Eq. (6). It is apparent that the pure ionization (PI) cross section is given by the term for k = 0;

$$\sigma_{PI}(n,j) = 2\pi P_{Mn}(0) \int_0^\infty [p_{LI}(b)]^j[1 - p_{LC}(b) - p_{LI}(b)]^{J-j}bdb \quad (7)$$

Similarly, the cross section for ionization accompanied by one-electron capture is given by the term for k = 1

$$\sigma_{1C}(n,j) = 2\pi P_{Mn}(0) \int_0^\infty jp_{LC}(b)[p_{LI}(b)]^{j-1} \times [1 - p_{LC}(b) - p_{LI}(b)]^{J-j}bdb \quad (8)$$

and the cross section for ionization accompanied by two-electron capture is given by the term for k = 2

$$\sigma_{2C}(n,j) = 2\pi P_{Mn}(0) \int_0^\infty (1/2)j(j+1)[p_{LC}(b)]^2[p_{LI}(b)]^{j-2} \times [1 - p_{LC}(b) - p_{LI}(b)]^{J-j} bdb \ , \qquad (9)$$

and so on.

The pure ionization cross section represented by Eq. (7) has been examined previously[7] and hence the present discussion will be limited to the one- and two-electron capture processes. In calculating the cross sections by means of Eq. (8) and Eq. (9), the L-shell ionization and capture probabilities were represented by the exponential functions

$$\begin{aligned} p_{LI}(b) &= p_{LI}(0)\exp(-b/r_I) \\ p_{LC}(b) &= p_{LC}(0)\exp(-b/r_C) \end{aligned} \qquad (10)$$

and the values for $p_{MI}(0)$, $p_{LI}(0)$ and $p_{LC}(0)$ were obtained using Olsen's CTMC code.[2] The radius parameters $r_I$ and $r_C$ were determined by fitting the total cross sections for one-electron capture to the experimental data.[8]

In order to predict the charge state distributions of the recoil ions, it is necessary to sum all the cross sections that contribute to each charge state. In the present calculations, it was assumed that each L-vacancy decayed 100% by single (LMM) Auger emission as long as there were sufficient numbers of electrons left in the M-shell. The contributing cross sections for each recoil-ion charge state produced in one-electron capture and two-electron capture collisions are listed in

Tables 1 and 2, respectively.

The calculated charge state distributions for Ar recoil-ion production in one-electron capture collisions with 1 MeV/amu $O^{q+}$ ions are compared with the experimental measurements in Fig. 1. Reasonably good agreement is achieved for $q > 3$. The poor agreement for $q = 3$ may indicate that multiple Auger processes cannot be neglected for collisions that produce low average recoil-ion charges, as has been suggested by Levin et al.[6] For example, when an Ar L-vacancy decays in the presence of a full M-shell, the probability of single Auger decay is 65%, of double Auger decay is 32%, and of triple Auger decay is 3%.

Table 1. Cross sections $\sigma(m\ell)$ that contribute to the production of Ar recoil-ions via one-electron capture accompanied by ionization and Auger multiplication, where m is the number of M-shell vacancies and $\ell$ is the number of L-shell vacancies.

| Recoil-ion charge | Contributing cross sections |
|---|---|
| 2 | (0,1) |
| 3 | (1,1) |
| 4 | (2,1),(0,2) |
| 5 | (3,1),(1,2) |
| 6 | (4,1),(2,2),(0,3) |
| 7 | (5,1),(3,2),(1,3) |
| 8 | (6,1),(4,2),(2,3),(0,4) |
| | (7,1),(5,2),(3,3),(1,4) |
| 9 | (8,1),(6,2),(4,3),(2,4),(0,5) |
| | (7,2),(5,3),(3,4),(1,5) |

Table 2. Cross sections $\sigma(m\ell)$ that contribute to the production of Ar recoil-ions via two-electron capture accompanied by ionization and Auger multiplication, where m is the number of M-shell vacancies and $\ell$ is the number of L-shell vacancies.

| Recoil-ion charge | Contributing cross sections |
|---|---|
| 4 | (0,2) |
| 5 | (1,2) |
| 6 | (2,2),(0,3) |
| 7 | (3,2),(1,3) |
| 8 | (4,2),(2,3),(0,4) |
| | (5,2),(3,3),(1,4) |
| 9 | (6,2),(4,3),(2,4),(0,5) |
| | (7,2),(5,3),(3,4),(1,5) |
| 10 | (8,2),(6,3),(4,4),(2,5),(0,6) |
| | (7,3),(5,4),(3,5),(1,6) |

However, the importance of double and triple Auger processes decreases rapidly as the number of M-shell vacancies produced in the collision increases.

The calculated and experimental charge state distributions for Ar recoil-ion production in two-electron capture collisions with 1 MeV/amu $O^{q+}$ ions are compared in Fig. 2. In this case, rather good agreement is achieved for all q. It should be noted that the cross sections for the two-electron capture charge state distributions were calculated using the same radius parameters (Eq. (10)) as were determined by fitting to the total one-electron capture cross sections. In view of this fact,

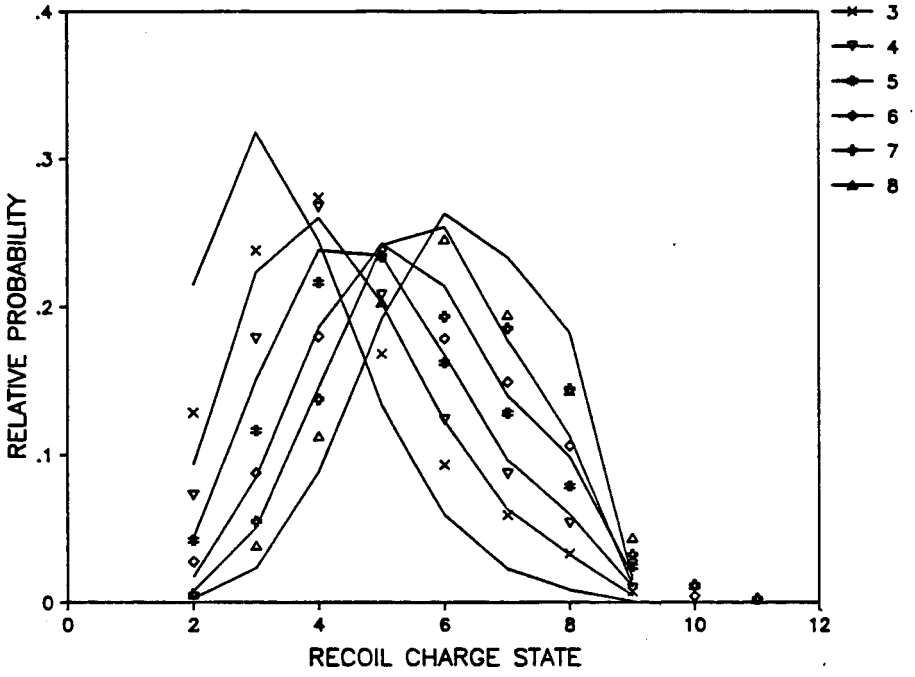


Figure 1. Comparison of the calculated and measured recoil-ion charge state distributions for one-electron capture.

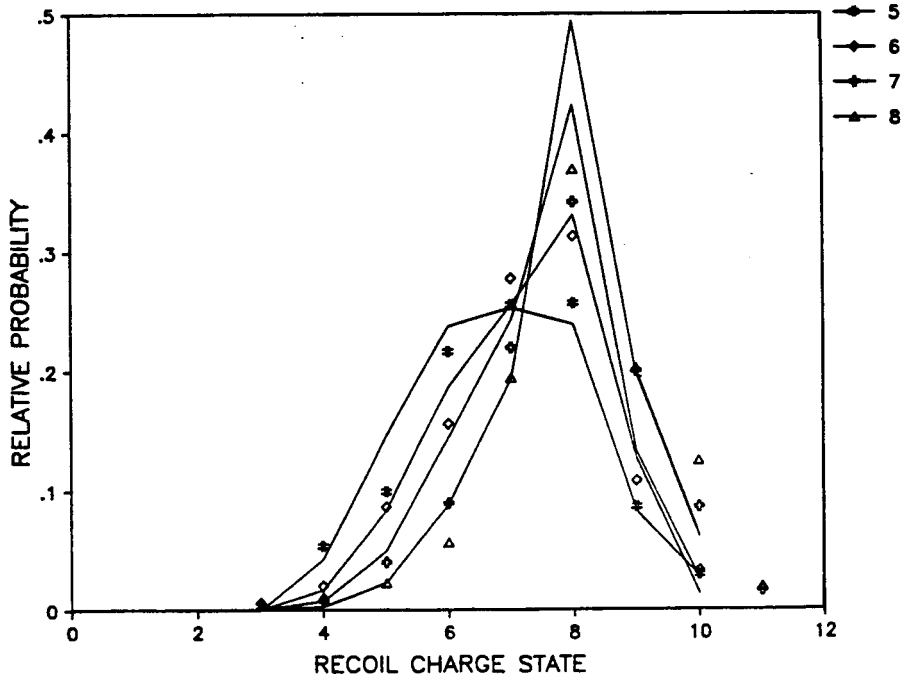


Figure 2. Comparison of the calculated and measured recoil-ion charge state distributions for two-electron capture.

the good agreement between the calculated and experimental charge state distributions in Fig.2 is especially gratifying.

Presented in Tables 3 and 4 are the mean recoil-ion charges for each of the charge state distributions. Listed in the last two columns of these tables are the mean recoil-ion charges predicted by the present model and by CTMC calculations. The latter were performed without inclusion of the L-shell ionization contribution (i.e. assuming $p_{LI}$ is negligible compared to $p_{LC}$), but additional vacancies resulting from Auger decay associated with L-electron capture were taken into account. This comparison illustrates the importance of L-shell ionization plus subsequent Auger decay as a mechanism for charge state multiplication. It is apparent that the two methods converge to the same mean charge state at high q where the L-shell ionization cross section becomes very small.[7]

It has been demonstrated that the charge state distributions for collisions involving the capture of one- or two-electrons and the ionization of many additional electrons are reasonably well described by the IEA, as long as care is taken to account for the charge multiplication associated with the Auger decay of L-shell vacancies. In the present model, a very simple parameterization of the ionization and capture probabilities in terms of exponential functions of the impact parameter led to good agreement with the experimental results. A more stringent test must await the availability of better theoretical estimates of the ionization and capture probabilities for fast heavy-ion collisions.

Table 3. Mean charges of recoil-ions produced in one-electron capture collisions.

| Projectile charge | Experiment | Present model | CTMC |
|---|---|---|---|
| 3 | 4.2 ± 0.3 | 3.61 | 3.18 |
| 4 | 4.65 ± 0.3 | 4.38 | 3.84 |
| 5 | 5.18 ± 0.3 | 4.91 | 4.40 |
| 6 | 5.5 ± 0.2 | 5.45 | 5.03 |
| 7 | 5.9 ± 0.2 | 5.72 | 5.58 |
| 8 | 6.1 ± 0.2 | 6.19 | 6.11 |

Table 4. Mean charges of recoil-ions produced in two-electron capture collisions.

| Projectile charge | Experiment | Present model | CTMC |
|---|---|---|---|
| 5 | 6.9 ± 0.3 | 6.74 | 6.34 |
| 6 | 7.2 ± 0.2 | 7.18 | 6.89 |
| 7 | 7.9 ± 0.2 | 7.42 | 7.32 |
| 8 | 8.1 ± 0.2 | 7.75 | 7.71 |

REFERENCES

1. T. J. Gray, C. L. Cocke, and E. Justiniano, Phys. Rev. A22, 849 (1980).

2. A. Muller, B. Schuch, W. Groh, E. Salzborn, H. F. Beyer, P. H. Mokler, and R. E. Olson, Phys. Rev. A33, 3010 (1986).

3. P. Richard, J. Ullrich, S. Kelbch, H. Schmidt-Bocking, R. Mann, and C. L. Cocke, Nucl. Instr. Meth. A240, 532 (1985).

4. J. H. McGuire, and L. Weaver, Phys. Rev. A16, 41 (1977).

5. M. Horbatsch, J. Phys. B: At. Mol. Phys. 19, L193, (1986).

6. J. C. Levin, C. S. O, H. Cederquist, C. Biedermann, and I. A. Sellin, Phys. Rev. A38, 2674 (1988).

7. O. Heber, G. Sampoll, B. B. Bandong, R. J. Maurer, E. Moller, R. L. Watson, I. Ben-Itzhak, J. L. Shinpaugh, J. M. Sanders, L. Hefner, and P. Richard (to be published in Phys. Rev A).

8. O. Heber, G. Sampoll, R. J. Maurer, B. B. Bandong, and R. L. Watson, to be published in Nucl. Instr. Meth. B.

B. Charge State Distributions of He, Ne, and Ar Recoil-Ions Produced in Collisions by 10 to 30 MeV/u $N^{7+}$ Ions

(O. Heber, B. B. Bandong, G. Sampoll, and R. L. Watson)

The first Born Approximation (BA) provides a good description of the single ionization process for fast ion-atom collisions where the velocity of the projectile is much greater than the velocity of the target electron. The double ionization process, on the other hand, is much harder to describe because it is very sensitive to the influence of electron-electron correlation.[1] When electron correlation effects are small, the process may be described in terms of double collisions by the projectile using the IEA, and the double ionization probabilities are expressed as products of single ionization probabilities[2,3]. This mechanism will be referred to as TS2.[1]

When electron correlation effects are large, the double ionization process may better be described in terms of a single collision between an electron and the projectile, along with a post-collision interaction between the two electrons.[1] This mechanism will be referred to as TS1. At high velocities, TS1 should become independent of projectile velocity.

A third mechanism that contributes to double ionization is the shakeoff process (SO). In shakeoff, the first electron is ejected by the projectile while the second electron is ejected as a result of the sudden change in the effective nuclear potential caused by the removal of the first electron. The shakeoff probability also should be independent of projectile velocity.[4]

Previous measurements employing electrons, protons and antiprotons on He targets[5-8] have established that the ratio of double- to single-ionization cross sections, $R_{2/1}$, decreases rapidly with increasing projectile velocity and becomes constant above 5 to 10 MeV/amu. Data for Ne and Ar targets display a similar behavior, although the value of the high energy limit is different than that for protons and electrons[1].

As indicated above, the projectile velocity independence of $R_{2/1}$ suggests that the IEA should not be applicable to high velocity collisions, which is indeed the case for low Z projectiles such as protons and alpha particles. However, it has been demonstrated that the IEA does provide cross sections which are in good agreement with high velocity data for highly stripped uranium (i.e. 430 - 955 MeV/amu $U^{q+}$ where q = 68 to 90).[9,10] Thus, it would appear that the dominant high velocity double ionization mechanism must change from TS1 to TS2 as the projectile charge increases.

We are to utilizing the capabilities of the new Texas A&M K500 superconducting cyclotron to study the velocity dependence of multiple ionization by low Z projectiles in the 10 to 80 MeV/u region. In the experiments presented here, beams of $N^{3+}$ and $N^{4+}$ having energies ranging from 10 to 30 MeV/u were extracted from the cyclotron and passed through a stripping foil. Fully stripped $N^{7+}$ ions were selected by means of a bending magnet and directed through a differentially pumped gas cell to a surface barrier detector. The recoil ions were accelerated out of the gas cell by a constant electric field and detected by a chevron microchannel plate assembly. Charge state identification of the recoil-ions was accomplished by time-of-flight (TOF) analysis.[11] The target gas

pressure was maintained at approximately 1 mTorr to assure single collision conditions.

Typical TOF spectra for He, Ne, and Ar recoil-ions produced by 10 MeV/u $N^{7+}$ are shown in Fig. 1. The relative probabilities for the production of the various charge states were determined from their relative intensities in the TOF spectra. The ratio of the probability for $He^{2+}$ production to that for $He^{1+}$ production ($R_{2/1}$) obtained in the present experiments is shown plotted as a function of the squared projectile velocity in Fig. 2. The nitrogen data at 1.4 and 2.3 MeV/u are from Refs. 12 and 5, respectively. Also shown for comparison in this figure are other experimental results for protons, antiprotons, and electrons.[1] The ratios obtained with nitrogen ions ions appear to level off at a value of 0.012 ← 0.002, about five times larger than the limit established by the proton, antiproton, and electron data.

Based upon the expectation that the high velocity behavior of $R_{2/1}$ is dictated by the SO mechanism, McGuire[2] has predicted that $R_{2/1}$ should reach a constant value which is independent of projectile charge. The solid line in Fig. 2 shows the predictions of a theoretical analysis of the velocity dependence of $R_{2/1}$ by Knudsen[5] using the Born approximation. The present results indicate that either the velocity at which $R_{2/1}$ becomes constant is much higher than 35 a.u. or a charge dependent mechanism contributes significantly to the double ionization cross section for high velocity nitrogen ions. It is possible that the TS2 mechanism, whose contribution to $R_{2/1}$ at high velocities varies as $Z_p^2/[v^2 \ln(Z_t/v)]$, will not be negligible over the range of velocities investigated with the higher $Z_p$ nitrogen projectiles. Therefore, it

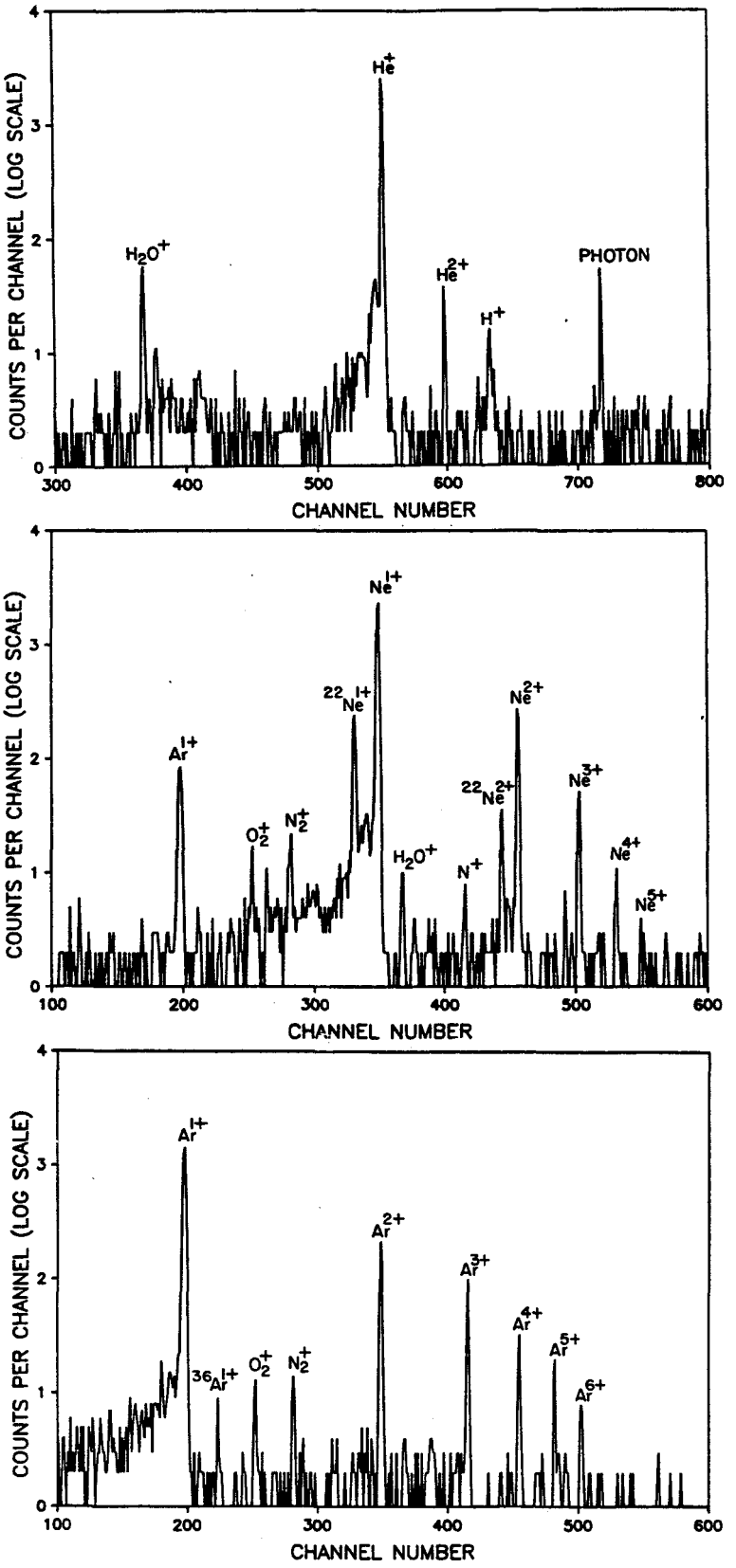


Figure 1. Time-of-flight spectra for (a) He, (b) Ne, and (c) Ar recoil ions produced in collisions with 10 MeV/u $N^{7+}$.

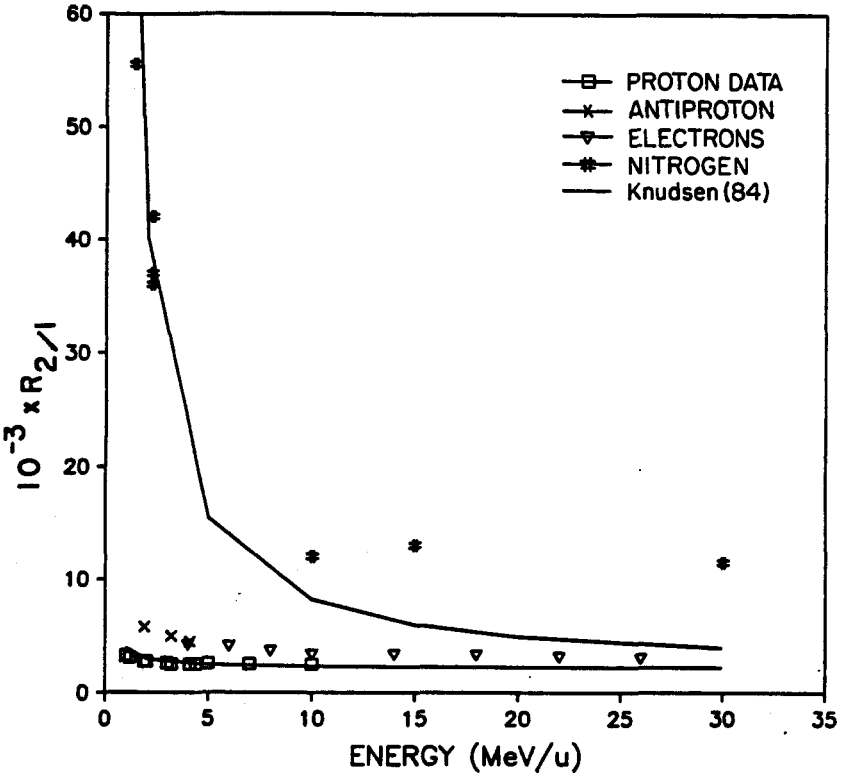


Figure 2. Comparison of the present double-to-single ionization ratios, $R_{2/1}$, for $N^{7+}$ ions with data for light ions and electrons.

will be important to extend these measurements to much higher velocities to see if the SO limit is eventually reached.

The charge state production probabilities are shown in Figs. 3 and 4 for Ne and Ar targets, respectively, along with data points for 1.4 MeV/u $N^{6+}$ on Ne and $N^{7+}$ on Ar from Ref. 12. It is apparent from this data that the probabilities become constant above a velocity of approximately 20 a.u. The solid lines in Figs. 3 and 4 show the results of IEA calculations employing the same type of exponential probability functions as described in section D of this report. These probability functions were fitted to single ionization cross sections that had been normalized to the well known asymptotic $\ln(v)/v^2$ velocity dependence. The disagreement between the model calculations and the experimental

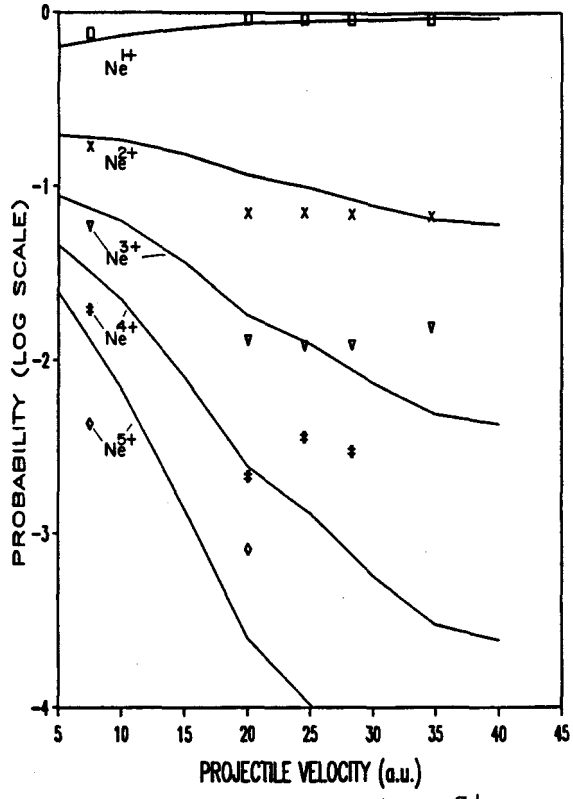


Figure 3. Relative probabilities for $Ne^{q+}$ production in $N^{7+}$ collisions. The data at v ≈ 7.5 a.u. ($N^{6+}$) is from Ref. 12.

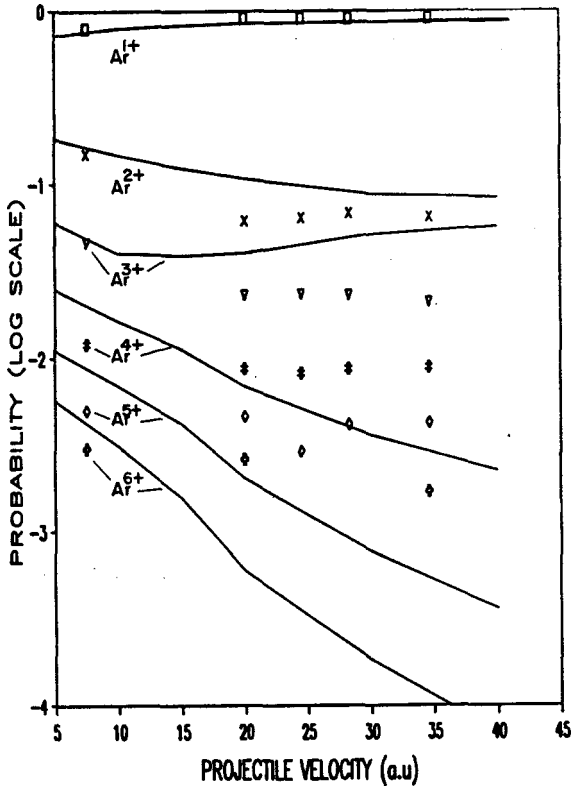


Figure 4. Relative probabilities for $Ar^{q+}$ production in $N^{7+}$ collisions. The data at v ≈ 7.5 a.u. is from Ref. 12.

results becomes larger with increasing velocity and this shows that the velocity independence of the data in the high velocity region must be attributed to some mechanism other than TS2.

The above findings suggest that the TS1 mechanism may play a dominant role at high velocities. In the TS1 mechanism, the "first" electron to be ejected may collide with other electrons in the near vicinity, causing them to be ejected. Calculations and measurements[14] at lower energies lead to the conclusion that the average energy of an ejected electron is about 200 eV. It is likely that at higher velocities, where the TS2 mechanism is not dominant, the first electron will be ejected with much more than the average energy, thereby enhancing its probability for ejecting other electrons on the way out of the target atom. The electron energy distribution does not vary much with the projectile velocity, but it is very sensitive to the projectile charge. This characteristic would explain the larger asymptotic probability ratios observed with higher q projectiles.

The classical limit for energy transfer to a quasifree electron requires that the final velocity of the electron be less than twice the velocity of the projectile. Thus, it is to be expected that the electron energy will eventually peak at the classical limit and become independent of q. On the other hand, the TS2 mechanism depends on $q^2$, and hence may become the dominant ionization mechanism in the high velocity region beyond some value of q. This may explain why the IEA apparently works for high velocity, highly-charged uranium ions.[9,10].

**References**


1. L. H. Andersen, P. Hvelplund, H. Knudsen, S. P. Moller, A. H. Sorensen, K. Elsener, K.-G. Rensfelt, and E. Uggerhoj, Phys. Rev. A36, 3612 (1987).

2. J. H. McGuire, Phys. Rev. Lett. 49, 1153 (1982).

3. J. H. McGuire and L. Weaver, Phys. Rev. A16, 41 (1977).

4. T. A. Carlson, Phys. Rev. 156, 142 (1967).

5. H. Knudsen, L. H. Andersen, P. Hvelplund, G. Astner, H. Cederquist, H. Danared, L. Liljeby, and K.-G. Rensfeld, J. Phys. B17, 3545 (1984).

6. M. B. Shah and H. B. Gilbody, J. Phys. B18, 899 (1985).

7. R. D. DuBois, S. T. Manson, Phys. Rev. A35, 2007 (1987).

8. A. Muller, W. Groh, U. Kneissl, R. Heil, H. Stroher, and E. Salzborn, J. Phys. B16, 2039 (1983).

9. S. Kelbch, J. Ullrich, W. Rauch, H. Schmidt-Bocking, M. Horbatsch, R. M. Dreizler, S. Hagmann, R. Anholt, A. S. Schlachter, A. Muller, P. Richard, Ch. Stoller, C. L. Cocke, R. Mann, W. E. Meyerhof, and J. D. Rasmussen, J. Phys. B19, L47 (1986).

10. W. E. Meyerhof, R. Anholt, X. Xu, H. Gould, B. Feinberg, R. J. McDonald, H. E. Wegner, and P. Thieberger, Phys. Rev. A35, 1967 (1987).

11. R. J. Maurer, C. Can, and R. L. Watson, Nucl. Instr. Meth. B27, 512 (1987).

12. A. Muller, B. Schuch, W. Groh and E. Salzborn, Z. Phys. D7, 251 (1987).

13. O. Heber, G. Sampoll, B. B. Bandong, R. J. Maurer, E. Moler, R. L. Watson, I. Ben-Itzhak, J. L. Shinpaugh, J. M. Sanders, L. Hefner, and P. Richard (to be published in Phys. Rev. A ).

14. R. Schuch, H. schone, P. D. Miller, H. F. Krause, P. F. Dittner, S. Datz, and R. E. Olsen, Phys. Rev. Lett. 60, 925 (1988).

C. Studies of Recoil Ions Produced in Collisions of 40 MeV $Ar^{13+}$ with Atomic and Molecular Targets

(R. J. Maurer, C. C. Can and R. L. Watson)

In order to study electron capture processes in atomic and molecular gases, a post-collision charge state analyzer was added to our time-of-flight (TOF) system. The details of the TOF system have been discussed elsewhere.[1] Beam particles exiting the gas cell were charge state analyzed by an 8.2 kGauss magnet located 0.8 meters behind the gas cell. The charge separated beams were detected by a silicon surface barrier detector positioned 22 cm behind the magnet at a take-off angle of 60 degrees with respect to the beam axis. For an incident 40 MeV $Ar^{13+}$ beam, post-collision charges of +12, +11 and +10, could be easily resolved.

Using the post-collision charge state analyzer, the recoil ion charge state distributions for Ne and Ar were measured in coincidence with the post-collision charge states of an incident 40 MeV $Ar^{13+}$ beam. Presented in Fig. 1 are TOF spectra showing the recoil ion charge state distributions for Ne and Ar produced in collisions with 40 MeV $Ar^{13+}$ ions. Spectrum (a) contains the recoil ion charge state distribution resulting from direct ionization (DI). Spectra (b), (c) and (d) are the recoil ion charge state distributions produced when the projectile captured 1 (C1), 2 (C2) or 3 (C3) electrons, respectively.

Although the recoil ion charge state distributions produced by direct ionization of Ne and Ar are similar, considerably higher average charge states are produced following electron capture in Ar than in Ne.

It is clear in both cases that electron capture by the projectile is accompanied by simultaneous multiple ionization of the recoil ion. For one- and two-electron capture events in Ne, the average recoil ion charges are +4.1 and +5.6, respectively, whereas for one-, two- and three-electron capture events in Ar, the average recoil ion charges are

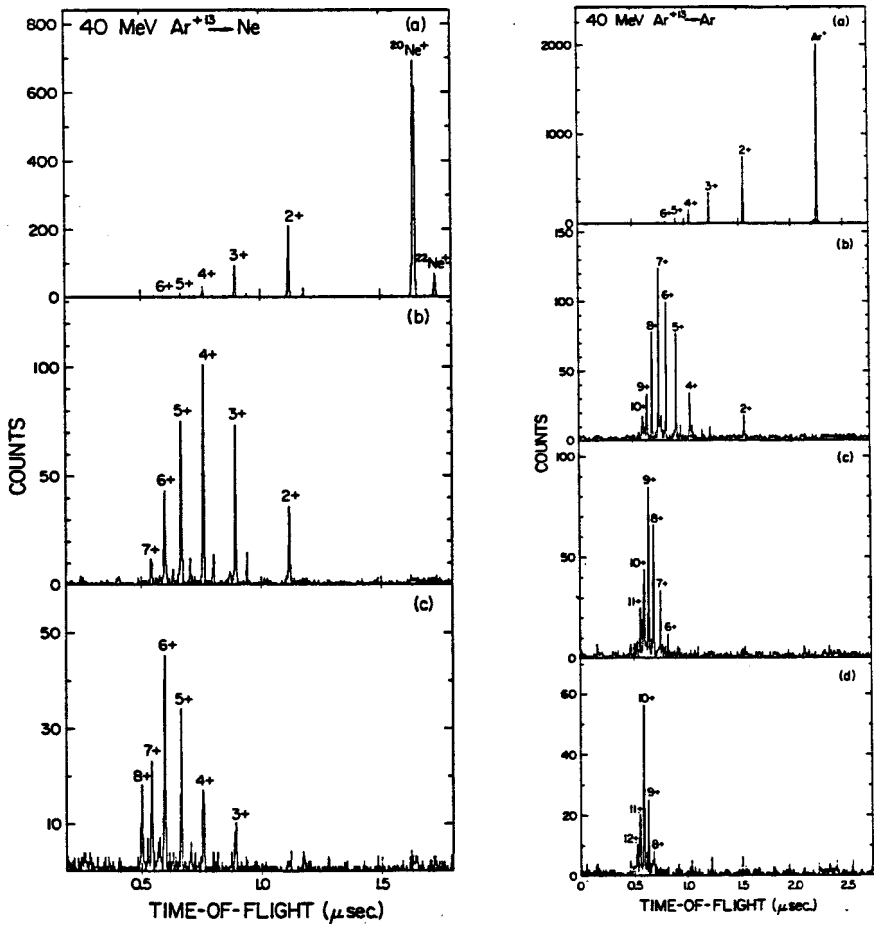


Figure 1. Time-of-flight spectra of Ne and Ar recoil ions produced by 40 MeV $Ar^{13+}$ projectiles undergoing a) direct ionization, and b-d) one, two and three electron capture, respectively.

+6.4, +8.9, and +10.1, respectively.

The Ne and Ar recoil ion production cross sections for direct ionization, one-electron capture, two-electron capture, and three-electron capture (argon only) by 40 MeV $Ar^{13+}$ impact are shown in Figs. 2 and 3. The solid lines in Figs. 2 and 3 were drawn through the data points from the present measurements to distinguish them from the other experimental and theoretical results. The Uncertainty in the absolute values of the cross sections from the present measurements is estimated to be of the order of 30%. The efficiency of the TOF spectrometer was determined by measuring TOF spectra of Ne and Ar recoil ions produced by 2.75 MeV $H^+$ impact and normalizing the relative yields to the absolute

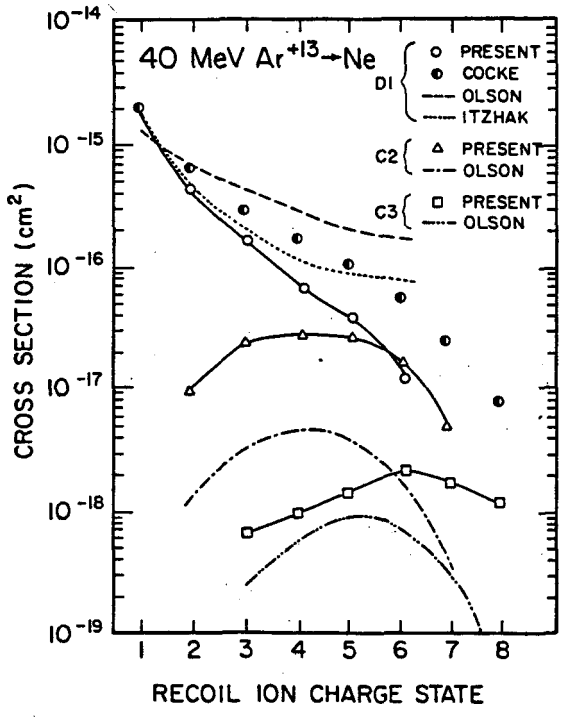


Figure 2. Cross sections for Ne recoil ion production via direct ionization (o), one-electron capture (Δ), and two-electron capture (□) by 40 MeV $Ar^{13+}$ ions.

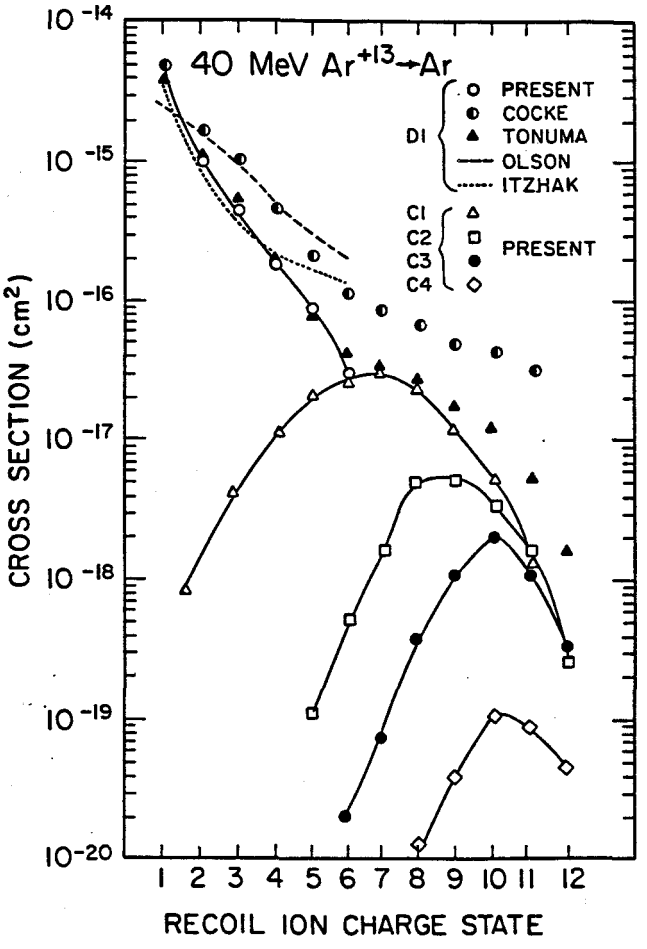


Figure 3. Cross sections for Ar recoil ion production via direct ionization (o), one-electron capture (Δ), two-electron capture (□), three-electron capture (o), and four-electron capture (◊) by 40 MeV $Ar^{13+}$ ions.

ionization cross sections measured by Wexler et al.[2] The efficiency of the TOF spectrometer was found to be 4.6% and was assumed to be constant for all charge states.

The present cross sections for recoil ion production by direct ionization are compared to those reported by Cocke[3] and Tonuma[4]. It should be noted that the cross sections reported by Cocke are for $Cl^{12+}$ projectiles and that the cross sections from both of the above sources include contributions from electron capture as well as direct ionization,

since no post-collision charge state analysis of the beam was performed. These extra contributions should be negligible for the low charge states, but they become increasingly more important for the higher charge states. The cross sections reported by Tonuma for Ar are in good agreement with those measured in the present investigation, however, the cross sections reported by Cocke appear to be much too large for the higher charge states.

The experimental cross sections for direct ionization are compared with the results of the classical trajectory Monte Carlo method (CTMC) of Olson[5] and the semiclassical approximation of Itzhak[6] in Figs. 2 and 3. Both calculations greatly overestimate the cross sections for the higher charge states.

Little is known about electron capture by fast, highly-charged projectiles from molecules. Presented in Fig. 4 are the TOF spectra for fragment ions of $O_2$ produced in collisions with 40 MeV $Ar^{13+}$ projectiles following (a) direct ionization, (b) one-electron capture and (c) two-electron capture. The TOF spectrum for direct ionization is nearly identical to that obtained without post-collision charge state selection of the projectile. This is an indication that direct ionization is the dominate mechanism for producing the lower-charged atomic fragments from molecules. For one- and two-electron capture from $O_2$ (Ne), the average fragment ion charges were +2.7 (+4.1) and +3.9 (+5.6), respectively.

Electron rearrangement complicates the interpretation of the TOF spectrum of a molecule. For example, consider a small impact parameter collision between a 40 MeV $Ar^{13+}$ ion and an $O_2$ molecule, in which one electron is captured and three are ionized, leaving an $O_2^{4+}$ molecular

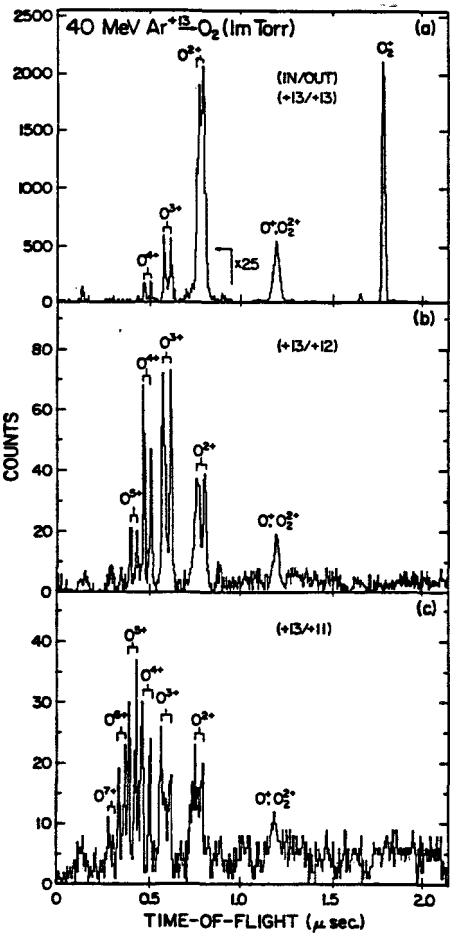


Figure 4. Fragment ion TOF spectra for $O_2$ produced by 40 MeV $Ar^{13+}$ ions undergoing a) direct ionization, b) one-electron capture, and c) two-electron capture.

ion. (This is the most probable charge state produced in such collisions with Ne atoms). Since electron capture requires a small impact parameter collision (on the order of the radius of the 2p shell in oxygen), and since the two atoms in $O_2$ have an equilibrium bond distance of 1.21 Å, most of the electron capture and ionization should occur from a single atom of the molecule. Following electron rearrangement in which some of the vacancies are transferred to the neighboring oxygen atom, the molecular ion dissociates, resulting in either a symmetric charge split (+2,+2) or an asymmetric charge split (+1,+3).

For two-electron capture, the average charge of the $O^{q+}$ fragments increases by only one unit over that for one-electron capture. As in the case of Ne, two-electron capture processes may proceed via several capture channels including a) capture of two L-shell electrons, b) capture of one L-shell electron and one K-shell electron and c) capture of two K-shell electrons. If K-capture occurs, however, the average charge will increase by one unit as a result of Auger decay. The relative contributions of each of these processes to the total cross section for double electron capture, however, cannot be determined from the TOF measurements alone.

The peaks corresponding to $q > 1$ in Fig. 4 are all split into doublets characteristic of very energetic recoil ions. The peak splitting has been used to extract average kinetic energies for the fragment ions produced in molecular dissociation. Presented in Table 1 are the kinetic energies determined for $O^{q+}$ fragments produced by 40 MeV $Ar^{13+}$ ions undergoing (a) direct ionization, (b) one-electron capture and (c) two-electron capture. Also included in table 1 are the calculated kinetic energies for point charges initially separated by the equilibrium bond distance (1.21 Å). The measured and calculated kinetic energies for the indicated dissociation pathways are in good agreement. It is apparent from spectra (a) and (b) in Fig. 4 that the splitting for the $O^{2+}$ and $O^{3+}$ peaks is noticably larger for electron capture than for direct ionization. This indicates that the dissociation channels for the production of $O^{2+}$ and $O^{3+}$ ions are different for the two cases. Direct ionization favors the (q/q-1) dissociation channel, whereas, electron capture favors the (q/q) and (q/q+1) channels. This simply

reflects the fact that single electron capture is accompanied by the ionization of several electrons resulting in much higher stages of ionization than are produced by direct ionization. For double electron capture, atomic oxygen fragments having charges up to +5 and kinetic energies up to 157 eV/ion were detected from the dissociation of molecular ions having charge states as high as +10.

TABLE 1. Kinetic energies (eV) for $O^{q+}$ fragments from $O_2$.

| | Fragment | $E_k$ | $E_k$ (calc.) | Dissociation Path |
|---|---|---|---|---|
| DI | $O^{2+}$ | 10.4±0.5 | 11.9 | $O_2^{3+} \longrightarrow O^{2+} + O^{+}$ |
| | $O^{3+}$ | 38.6±2.9 | 35.8 | $O_2^{5+} \longrightarrow O^{3+} + O^{2+}$ |
| | $O^{4+}$ | 97.9±8.9 | 95.4 | $O_2^{8+} \longrightarrow O^{4+} + O^{4+}$ |
| C1 | $O^{2+}$ | 28.0±0.5 | 23.8 | $O_2^{4+} \longrightarrow O^{2+} + O^{2+}$ |
| | | | 35.8 | $O_2^{4+} \longrightarrow O^{2+} + O^{3+}$ |
| | $O^{3+}$ | 60.1±1.3 | 53.7 | $O_2^{6+} \longrightarrow O^{3+} + O^{3+}$ |
| | | | 71.6 | $O_2^{6+} \longrightarrow O^{3+} + O^{4+}$ |
| | $O^{4+}$ | 100.5±4.2 | 95.4 | $O_2^{8+} \longrightarrow O^{4+} + O^{4+}$ |
| | $O^{5+}$ | 125.6±7.2 | 119.0 | $O_2^{9+} \longrightarrow O^{5+} + O^{4+}$ |
| C2 | $O^{4+}$ | 124.6±7.1 | 119.0 | $O_2^{9+} \longrightarrow O^{4+} + O^{5+}$ |
| | $O^{5+}$ | 157.0±9.0 | 149.0 | $O_2^{10+} \longrightarrow O^{5+} + O^{5+}$ |
| | $O^{6+}$ | 150.7±8.6 | 143.0 | $O_2^{10+} \longrightarrow O^{6+} + O^{4+}$ |

References

1. R. L. Watson and R. J. Maurer, Nucl. Inst. and Meth. A262, 99 (1987).

2. S. Wexler, J. Chem. Phys. 41, 1714 (1964).

3. C. L. Cocke, Phys. Rev. A20, 749 (1979).

4. T. Tonuma, H. Shibata, S. H. Be, H. Kumagai, M. Kase, T. Kambara, I. Kohno, A. Ohsake and H. Tawara, Phys. Rev. A33, 3047 (1986).

5. R. E. Olson, J. Phys. B: Atom. Molec. Phys. 12, 1843 (1979).

6. I. Ben-Itzhak (private communication).

D. Two-Fragment Coincidence Studies of the Breakup of Multicharged Molecular Ions Produced by Heavy Ion Impact (G. Sampoll, O. Heber, V. Horvat, and R. L. Watson)

We have obtained initial results from new, higher resolution two-fragment coincidence experiments on the dissociation of multicharged $O_2^{q+}$ molecular ions produced in collisions with 40 MeV $Ar^{13+}$ ions. Molecular ions were created in a differentially pumped collision cell and their dissociation products were accelerated out of the cell into a time-of-flight (TOF) spectrometer by means of a 1200 volt electrostatic potential (see fig. 1). In the TOF spectrometer, the fragment ions drifted through a 12 cm flight tube and were accelerated into a chevron microchannel plate (MCP) detector system.

A schematic diagram of the electronic system is shown in Fig. 2. In a given binary dissociation event, the first ion to reach the MCP generated a start signal for two time-to-amplitude converters (TAC 1 and TAC 2). A signal generated by the projectile ion in a surface barrier detector was delayed by 4 $\mu$s and used to stop TAC 1, thereby completing the flight time (t1) measurement of the first ion. When the second ion arrived at the MCP, it generated a stop signal for TAC 2, thereby completing the measurement of the flight time difference between ion 1 and ion 2 ($\Delta$t). Separate analog-to-digital converters (ADCs) were used to digitize the t1 and $\Delta$t analog signals from the two TACs, and this information was subsequently recorded on magnetic tape event-by-event, so as to maintain the correlation between the two times.

The TOF (t1) spectrum of the first ion to reach the detector, taken

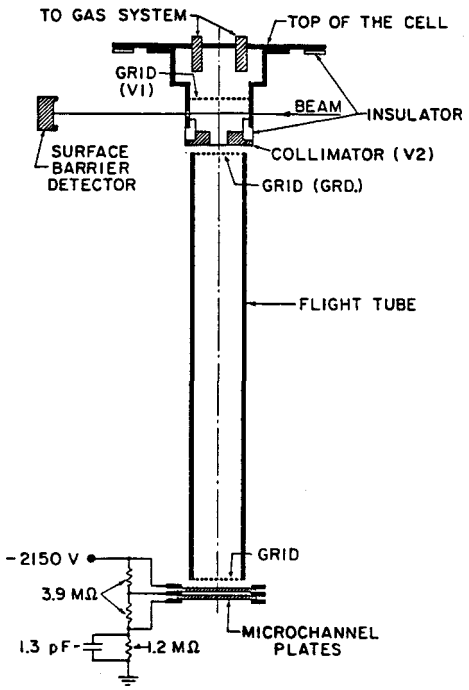


Figure 1. A diagram of the gas cell and TOF spectrometer.

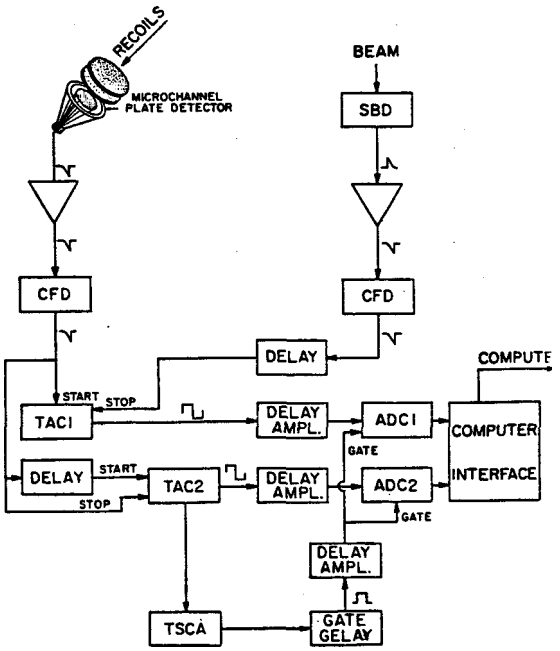


Figure 2. A diagram of the electronic system.

in coincidence with the second ion, is shown in Fig. 3. Off-line sorting of the Δt spectra was accomplished by placing windows around the peaks for the different ion charges in the TAC 1 spectrum (Fig. 3) and plotting histograms of the coincident Δt events. The Δt spectra generated by placing windows around the $O^{1+}$, $O^{2+}$, $O^{3+}$, and $O^{4+}$ peaks in the t1 spectrum are shown in Fig. 4. The structural features are labeled by the charges of the associated ion pairs. For example, the structure centered around 400 nsec in spectrum (b) of Fig. 4 is the distribution of Δt events for the case of an $O_2^{3+}$ molecular ion dissociating into an $O^+$ and an $O^{2+}$ ion. This structure actually consists of two distributions - one for dissociation events in which the initial trajectories of the $O^{2+}$ ions are in the downward direction (i.e. toward the flight tube) and one for dissociation events in which the

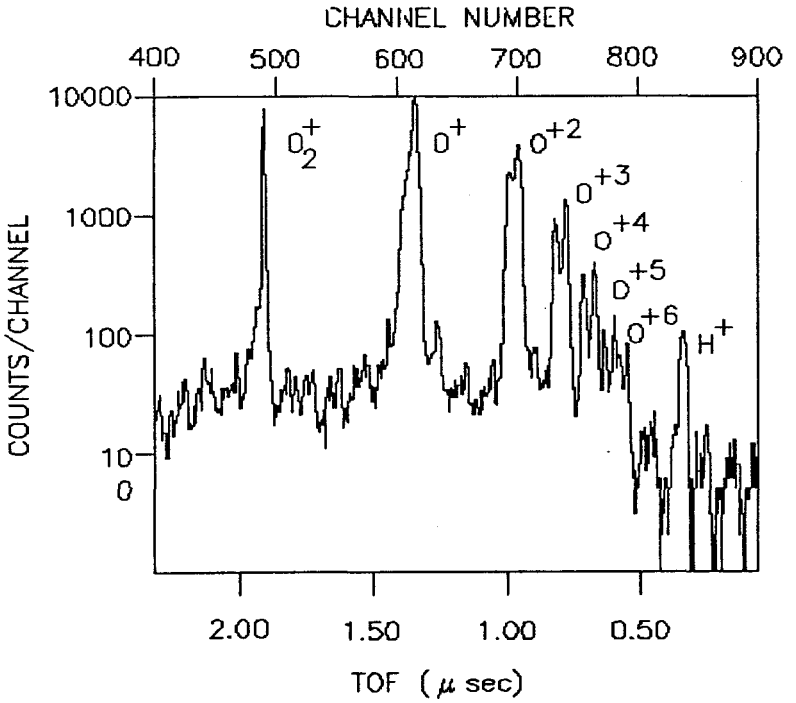


Figure 3. TOF (t1) spectrum of the first ion from the dissociation of $O_2$ molecular ions measured in coincidence with the second ion.

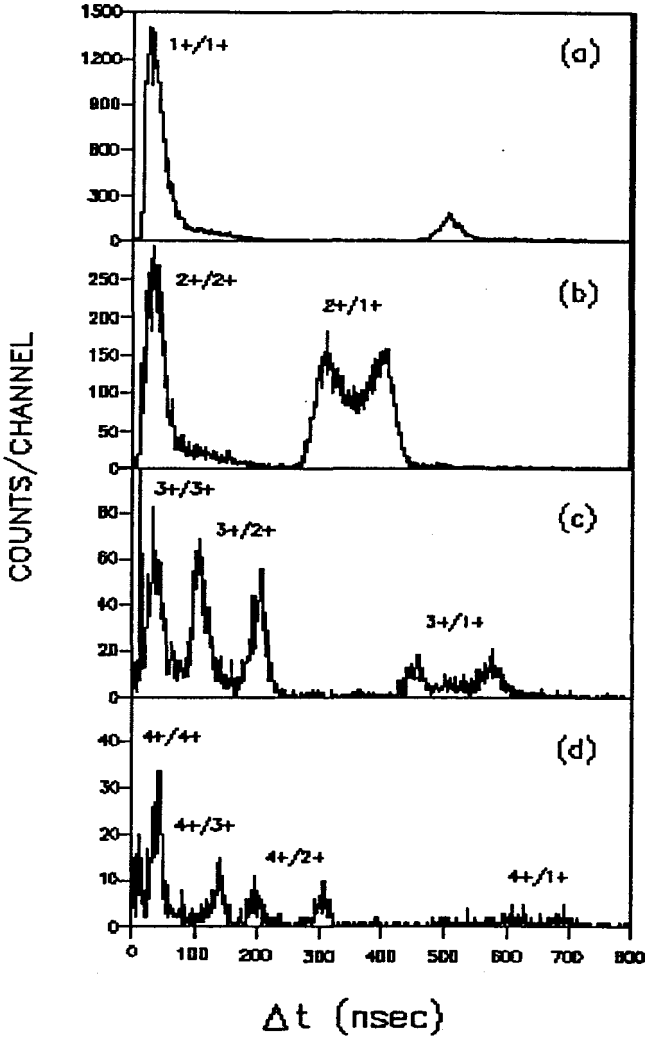


Figure 4. Sorted Δt spectra for ion pair coincidences. The structural features are labeled by the charges of the associated ion pairs.

initial trajectories of the $O^{2+}$ ions are in the upward direction. In either case, the $O^{2+}$ ion is the first to arrive at the MCP because its acceleration in the electric field is greater than that for the $O^{+}$ ion as a consequence of its larger charge.

An accurate translation of the Δt distributions into kinetic energy distributions requires a detailed simulation of the ion trajectories inside the gas cell and through the TOF spectrometer. A Monte Carlo

procedure employing the electrostatic lens program SIMION[1] to calculate each ion trajectory has been designed to run on the Cyclotron Institute's VAX 11/780. The starting coordinates of the two ion trajectories within the beam cylinder (i.e. the center of mass of the molecule) are specified by the distance from the TOF spectrometer symmetry axis Y, the distance from the beam axis $\rho$, and the angle with respect to the YZ plane $\vartheta$, as shown in Fig. 5. The initial ion trajectories are specified by the angles $\Theta$ and $\varphi$. These five coordinates are generated using a uniform distribution of random numbers ranging from 0 to 1. All values of Y, $\vartheta$, and $\varphi$ are equally probable, however $\rho$ and $\Theta$ are distributed according to the probability functions

$$P(\rho) = 2B^{-2}\rho \qquad (1)$$

$$P(\Theta) = (1/2)\sin\Theta \ , \qquad (2)$$

where B is the radius of the beam cylinder. To generate a given

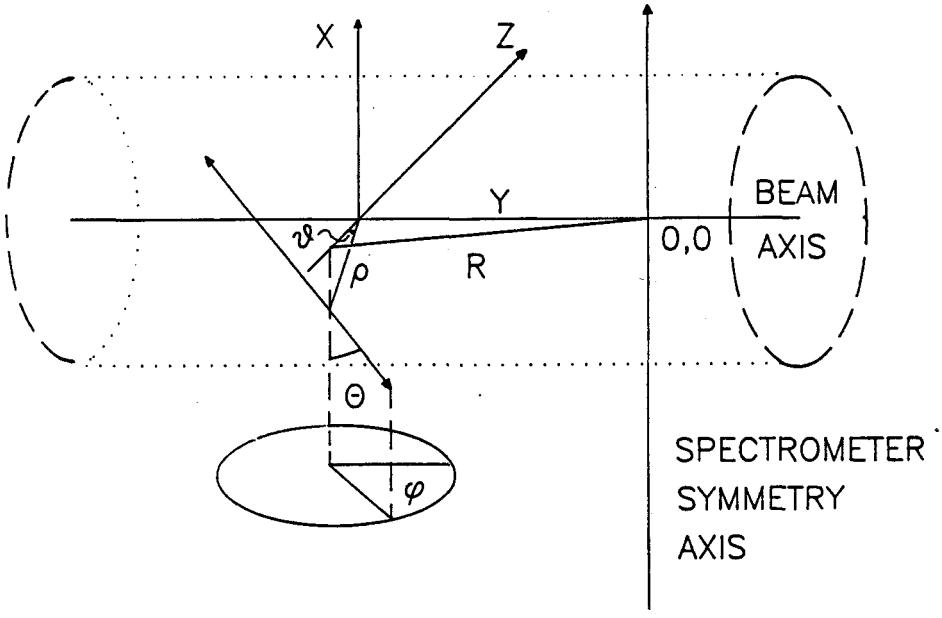


Figure 5. Coordinates used to calculate the simulated $\Delta t$ distributions.

probability distribution using a uniform distribution of random numbers, the following relationship is employed;

$$RN = \int_{x_{min}}^{x_{max}} P(x)dx \qquad (3)$$

where RN is a random number. Applying the above relationship to the probability functions (1) and (2) gives

$$\rho = (RN - B^2)^{-1/2} \qquad (4)$$

$$\theta = \cos^{-1}(1 - RN) \ . \qquad (5)$$

Once a set of starting coordinates has been picked, the radial (along R), tangential, and vertical (along X) velocity components are calculated. The radial and vertical velocity components are then sent to SIMION where the ion trajectories and flight times over small distance intervals are calculated. Because the SIMION program calculates trajectories only in the radial and vertical directions, new values of the radial and vertical coordinates must be calculated for each distance interval by taking into account the tangential velocity component. Summing the flight times over all the distance intervals from the starting point to the channel plate detector gives the total times of flight, from which $\Delta t$ for the ion pair is obtained.

Simulated time distributions for several different total kinetic energy releases (KERs) are compared with the experimental $\Delta t$ distribution for the breakup of $O_2^{2+}$ into two $O^{1+}$ ions in Fig. 6. A similar comparison for the breakup of $O_2^{3+}$ into an $O^{2+}/O^{1+}$ ion pair is shown in Fig. 7. The Coulomb potential energy of two point

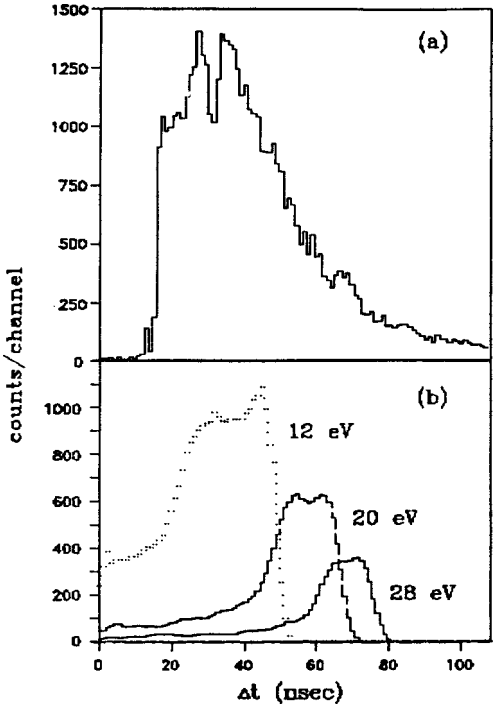


Figure 6. Comparison of the experimental Δt distribution for $O^{1+}/O^{1+}$ with simulated distributions for KERs of 12, 20, and 28 eV.

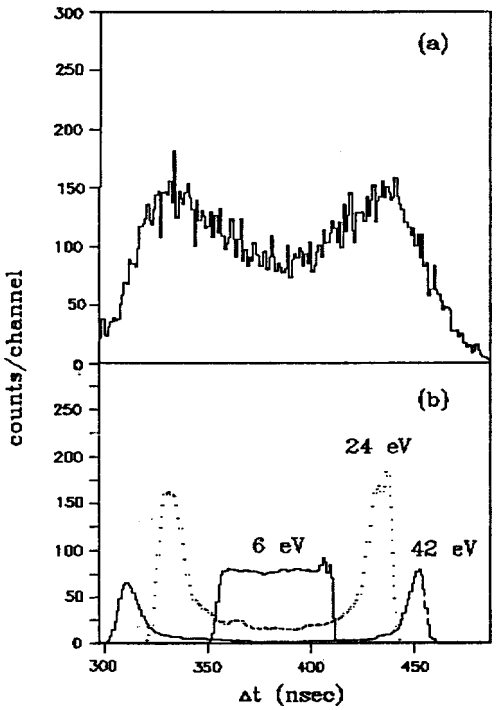


Figure 7. Comparison of the experimental Δt distribution for $O^{2+}/O^{1+}$ with simulated distributions for KERs of 6, 24, and 42 eV.

charges separated by the normal bond distance in $O_2$ (1.21 Å) is 11.9 eV. It is evident from Fig. 6 that the simulated time distribution for a KER corresponding to the Coulomb energy closely coincides with the highest intensity region of the experimental Δt distribution. The same is true for the $O^{2+}/O^{1+}$ distribution shown in Fig. 7, which has a Coulomb energy of 23.8 eV. By fitting simulated time distributions to the measured time distributions, it is possible to determine average values and widths of the kinetic energy distributions.

The experimental Δt distributions are considerably broader than the experimental resolution and show little evidence of real structure. This observation, together with the fact that the centroids of the Δt distributions closely correspond to the Coulomb energy positions, indicates that the excitation process may be viewed as a vertical transition from the $O_2$ ground state to a broad manifold of states located near the unscreened Coulomb potential. The absence of structure in the $O^{1+}/O^{1+}$ Δt distribution resulting from dissociative ionization by heavy ion impact is in contrast to the case of photodissociation, where structure attributed to the population of well defined metastable states in $O_2^{2+}$ has been observed.[2]

**References**

1. D. A. Dahl and J. E. Delmore, Idaho National Engineering Laboratory reportEGG-CS-7233 Rev. 1 (1987).

2. D. M. Curtis and J. H. D. Eland, Int. J. Mass Spectrom. and Ion Proc. **63**, 241 (1985).

E. Resonant Multielectron Transfer to Double K-Vacancy States in Oxygen Compounds (B. B. Bandong and R. L. Watson)

Significant chemical effects on the Kα hypersatellite structure of oxygen have been observed in the Ar-excited spectra of different oxides. In particular, certain peaks (e.g., the $K^2L^0$ peak in $CeO_2$, the $K^2L^1$ and $K^2L^2$ peaks in TiO) show highly enhanced intensities. The resonant electron transfer (RET) mechanism[1] has been applied in an attempt to account for the anomalous behavior of these peaks. The energy change associated with the electron transfer process has been calculated with corrections due to extra-atomic relaxation (the polarization energy) explicitly included. These corrections were found to be rather large for the double K-vacancy states of oxygen and hence it was important to include them in the analysis. The results provide evidence of multiple electron participation in the resonant transfer process and raise questions regarding the role of electron correlation.

Shown in Fig. 1 are the Kα hypersatellite spectra of oxygen obtained by bombarding thick target solid pellets of $K_2O$, BeO, CaO, SrO, and $CeO_2$ with 22 MeV C ions. The peaks are labeled according to the number of L-vacancies, n, in addition to the two K-shell vacancies ($K^2L^n$). The spectrum of $K_2O$ displays a rather symmetric intensity distribution centered between $K^2L^2$ and $K^2L^3$. In fact, its relative intensity distribution agrees well with a binomial distribution calculated using the experimental $p_L$ extracted from the spectrum. The shift of the intensity distribution towards the lower-order hypersatellite peaks for the more covalent BeO is consistent with a two-

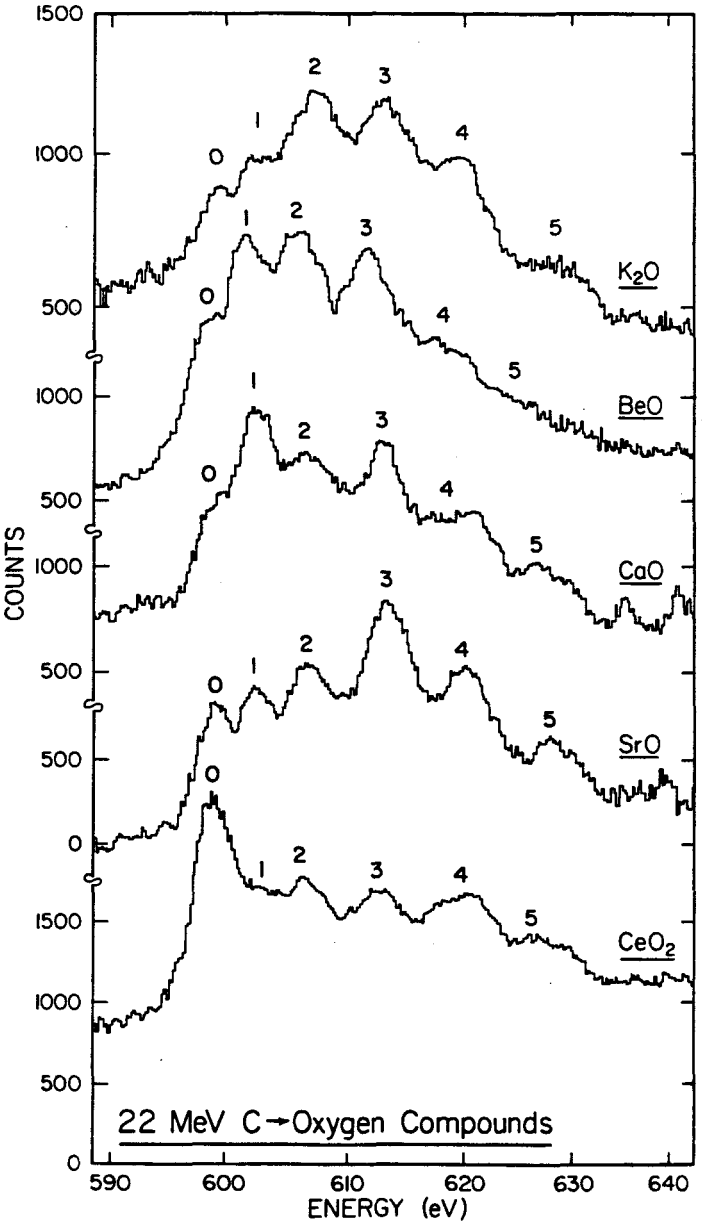


Figure 1. Kα hypersatellite spectra of oxygen in different oxides excited by 22 MeV C ions.

step mechanism, whereby the Rydberg levels (3s, 3p, 3d) of oxygen, after inner-shell ionization, descend and experience an energy level matching with the valence states of the metal. This level-matching condition allows for the transfer of electrons between the metal and the oxygen ion, leading to an effective population of M-levels in the excited $O^*$ atom. The oxygen M-electrons can cause $O^*$ LMM Auger transitions, thus

shifting the emission strength in the spectrum toward the lower-order hypersatellites.

The spectra of CaO, SrO, and $CeO_2$ exhibit several new features. Comparing CaO with $K_2O$, it is apparent that the $K^2L^1$ peak of the former is greatly enhanced while the $K^2L^2$ peak dips down in intensity. Likewise, for SrO the $K^2L^2$ peak is also suppressed in intensity; however, the $K^2L^0$ peak seems to have gained intensity while the $K^2L^1$ peak appears normal. In $CeO_2$, the $K^2L^0$ peak is greatly enhanced relative to the other hypersatellites peaks. The following reactions summarize one- and two- electron resonant transfer processes that can account for the above observations:

<u>CaO</u>:

$$Ca^{2+}(g.s.) + O^{2+}(1s^{-2}2p^{-2}) \underset{[K^2L^2]}{} = Ca^{3+}(3p^{-1}) + O^{+}(1s^{-2}2p^{-1}) \underset{[K^2L^1]}{} \quad (1a)$$

<u>SrO</u>:

$$Sr^{2+}(g.s.) + O^{2+}(1s^{-2}2p^{-2}) \underset{[K^2L^2]}{} = Sr^{4+}(4p^{-2}) + O^{o}(1s^{-2}) \underset{[K^2L^0]}{} \quad (1b)$$

<u>$CeO_2$</u>:

$$Ce^{4+}(g.s.) + O^{+}(1s^{-2}2p^{-}) \underset{[K^2L^1]}{} = Ce^{5+}(5p^{-1}) + O^{o}(1s^{-2}) \underset{[K^2L^0]}{} \quad (1c)$$

and/or,

$$Ce^{4+}(g.s.) + O^{2+}(1s^{-2}2p^{-2}) \underset{[K^2L^2]}{} = Ce^{6+}(5p^{-2}) + O^{o}(1s^{-2}) \underset{[K^2L^0]}{} \quad (1d)$$

When the energy change, $\Delta E$, associated with the reaction is zero, an electron or electron pair is free to transfer between the two ions, assuming any barrier separating them is low enough to be easily penetrated. In order to test the plausibility of this mechanism, the method for calculating $\Delta E$ formulated by Benka et al.[1] (which is based on

the point-charge model) was utilized. The polarization energy was obtained by means of the localized-hole point-ion (LHPI) model of Mahan.[2,3]

The results of this analysis applied to the alkaline earth oxides for the case of single RET to the $K^2L^2$ state of oxygen are shown in table 1. The $\Delta E$ was calculated with and without corrections for polarization energy, and the difference is observed to amount to as much as 10 to 15 eV. It can be seen that when $E_{rx}$ is included, the experimental observation is correctly predicted (enhanced $K^2L^1$ and suppressed $K^2L^2$ for CaO only).

Table 1. Calculated $\Delta E$ associated with the single RET process in alkaline earth oxides. The values for $\Sigma_2$ and $\Sigma_{ML}$ were taken from Mahan.[2,3] All values are given in eV.

Alk. earth oxides: $M^{2+}(g.s.) + O^{2+}(1s^{-2}2p^{-2}) = M^{3+}(np^{-1}) + O^{+}(1s^{-2}2p^{-1})$

| $M^{2+}$ (np) | $\Sigma_2(1)$ | $\Sigma_{ML}(1),O^{2-}$ | $\Sigma_{ML}(1),M^{2+}$ | $\Delta E$ without $E_{rx}$ | $\Delta E$ with $E_{rx}$ |
|---|---|---|---|---|---|
| $Mg^{2+}(2p)$ | 4.954 | 2.483 | 4.057 | 10.3 | 23.6 |
| $Ca^{2+}(3p)$ | 2.673 | 2.603 | 3.496 | -15.3 | -0.5 |
| $Sr^{2+}(4p)$ | 1.481 | 2.556 | 3.055 | -20.4 | -5.5 |
| $Ba^{2+}(5p)$ | 0.460 | 2.599 | 2.756 | -25.2 | -9.8 |

In the case of SrO, it is believed that the enhancement of the $K^2L^0$ peak comes from the the $K^2L^2$ state via a two-electron process. The $\Delta E$ value for this process is -1.5 eV ($E_{rx}$ included). If a single RET to the $K^2L^1$ state is postulated to account for the enhancement of the $K^2L^0$

peak, the calculated $\Delta E$ is 5.2 eV. Such a large $\Delta E$ value indicates that the single RET channel is energetically unfavorable. For $CeO_2$, the one-electron transfer process (1c) has a $\Delta E$ of 5.2 eV while the two-electron transfer process (1d) has a $\Delta E$ of 0.4 eV.

The oxygen K$\alpha$ hypersatellite spectra produced by 80 MeV Ar ion bombardment of a variety of solid oxides are shown in Fig. 2. In Fig. 2a, it is shown that oxides having the same crystal lattice structures and about the same ionicities yield nearly identical hypersatellite intensity distributions. However, the hypersatellite intensity distributions for the different structure groups are significantly different, as is shown in Fig. 2b. In Fig. 2c, spectra for three titanium oxides are compared with the spectra of other compounds having the same crystal structure, and large differences are observed. For example, consider the TiO/CaO comparison. Both of these oxides are highly ionic and of the rocksalt lattice structure. While the relative intensities of the $K^2L^3$, $K^2L^6$ and $K^2l^7$ peaks of these two spectra coincide quite well, the relative intensities of the $K^2L^1$, $K^2L^2$, $K^2L^4$ and $K^2L^5$ peaks do not. Such deviations could be caused by multiple-electron RET processes.

The results of calculations for various oxidation states of Ti are shown schematically in Fig. 3. In this figure, the initial (before transfer) and final (after transfer) states of oxygen are represented by energy levels labeled with the L-shell defect configuration. The number of electrons transferred to the O L-shell is given to the right of the final state of oxygen. Encircled numbers indicate energetically favorable resonances. Fig. 3(a) indicates that 3-electron transfer to

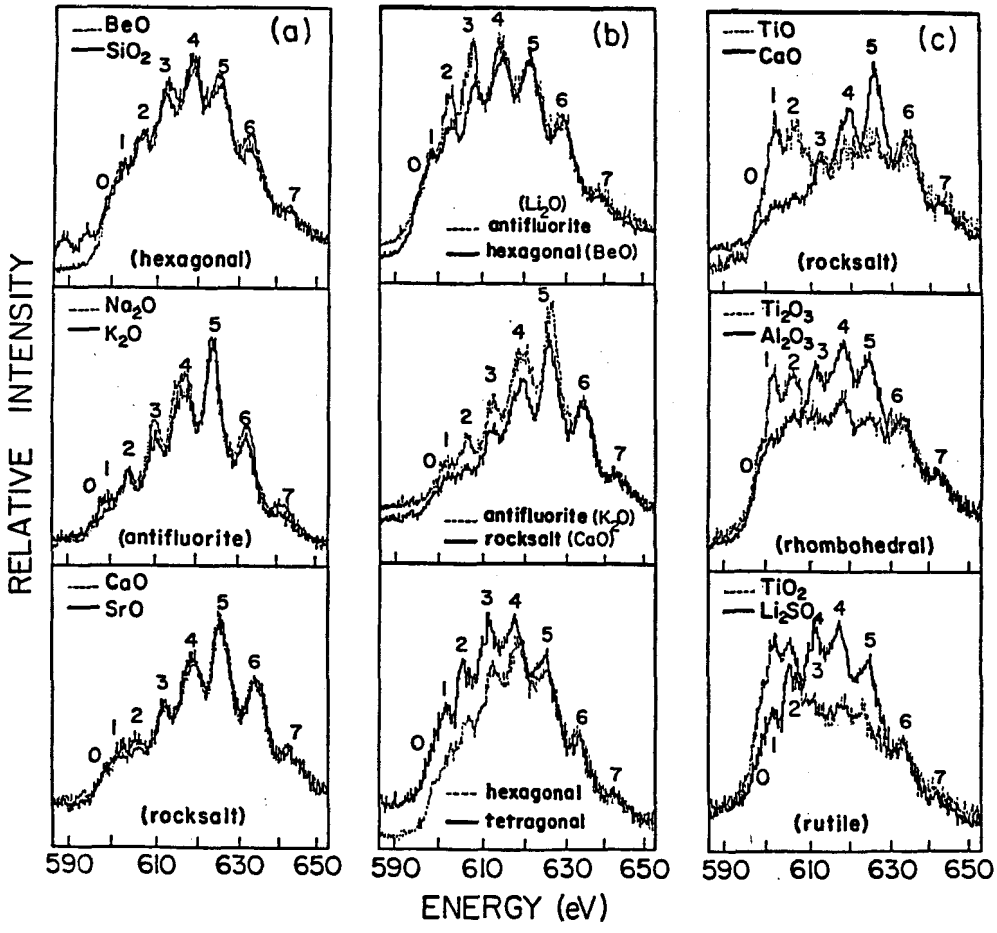


Figure 2. Comparisons of the Kα hypersatellite spectra of a variety of solid oxides, produced by 80 MeV Ar ion bombardment.

$K^2L^4$ (thereby enhancing the $K^2L^1$ peak intensity) and 1-electron transfer to $K^2L^3$ (thereby enhancing the $K^2L^2$ peak intensity) are resonance processes. Additional resonances involving 1-, 2-, and 4-electron

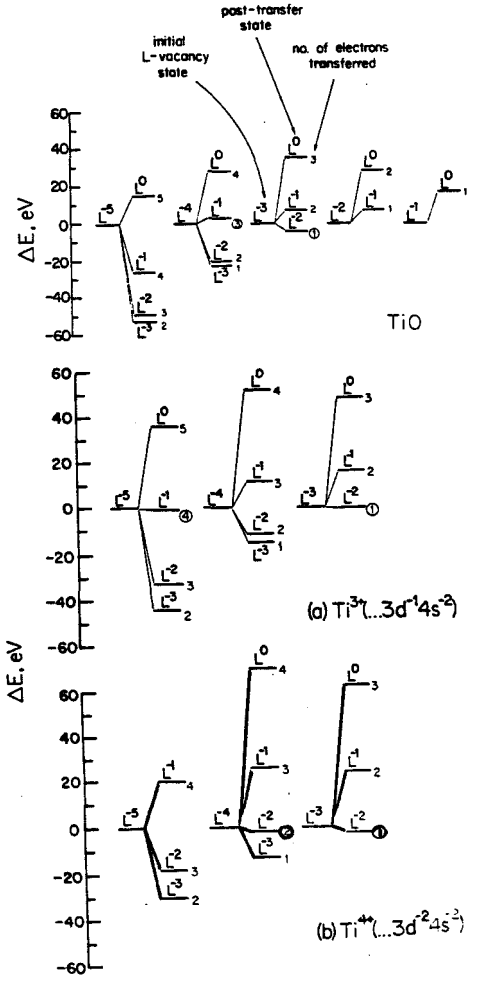


Figure 3. Schematic representation of the energy defect associated with the transfer of electrons from the 3p levels of (a) $Ti^{2+}$, (b) $Ti^{3+}$, and (c) $Ti^{4+}$ to the 2p levels of oxygen in different $K^2L^n$ defect configurations. (See text for further information).

transfer are identified in Fig. 3(b) and Fig. 3(c).

The model employed in this investigation explicitly assumes that the electrons are transferred in a correlated one-step manner. Correlated 2-electron transfer from a target atom to a projectile ion

has been observed in low energy collisions of $O^{6+}$ with He.[4] In this case, the resonance conditions were such that one electron was transferred to the 2p level and the other ended up in a Rydberg level having $n \geq 6$.

References:

1. O. Benka, R.L. Watson, and R.A. Kenefick, Phys. Rev. Lett. 47, 1202 (1981).

2. G. D. Mahan, Phys. Rev. B 21, 4791 (1980).

3. G. D. Mahan, Phys. Rev. B 22, 3102 (1980).

4. N. Stolterfoht, C. C. Havener, R. A. Phaneuf, J. K. Swenson, S. M. Shafroth, and F. W. Meyer, Phys. Rev. Lett. **57**, 74 (1986).

F. Collisional Quenching of $2^3P$ and $2^4P$ States in 33 MeV Two- and Three-Electron Mg Ions (G.-J. Yu, R. L. Watson, B. B. Bandong, C. Can, G. Sampoll, E. Moler and R. J. Maurer)

The spectra of Mg K$\alpha$ x-rays, emitted in collisions of 33 MeV Mg ions with noble gas atoms, have been measured using a curved-crystal spectrometer. Quenching of the metastable 1s2p $^3P$ state of He-like Mg and the 1s2$\ell$2p $^4P$ states of Li-like Mg caused the intensities of x-rays from these states to decrease, relative to the intensities of x-rays from the promptly-decaying $^1P$ and $^2P$ states, as the gas pressure increased. The $^1P/^3P$ and $^2P/^4P$ intensity ratios displayed large deviations from a linear dependence on pressure. It was proposed that contributions to the peaks associated with the metastable states from prompt spectator-electron transitions were the cause of the nonlinear pressure dependence, and this assertion was supported by measurements of the relative intensities of 2p-1s transitions from the most likely spectator-electron states.

Quenching cross sections were determined by fitting the observed pressure dependence of the x-ray intensity ratios to a function derived from the rate equation for the production and decay of these states, with additional terms to account for contributions from prompt spectator-electron transitions. The quenching cross sections obtained in this analysis are shown in Fig. 1.

The quenching cross sections were found to increase monotonically with increasing noble gas atomic number, and those for the $2^3P$ state were very nearly equal to the geometric cross section of the target

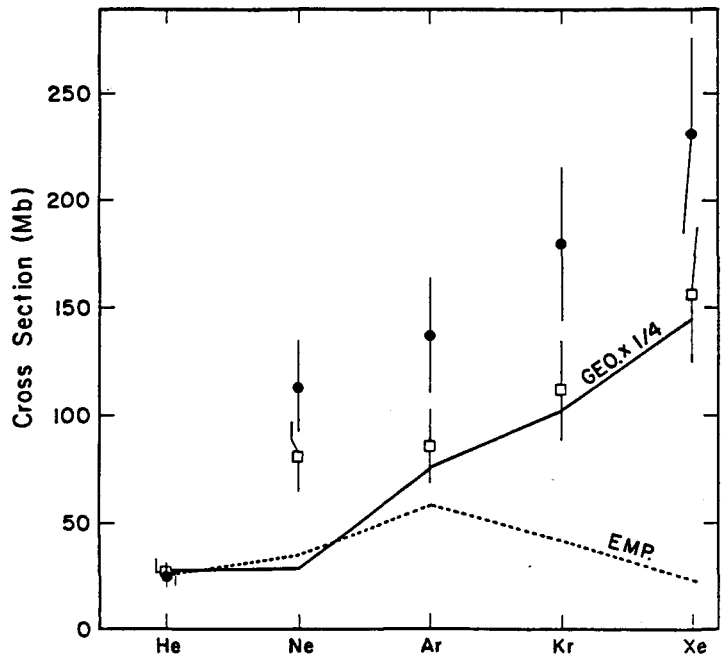


Figure 1. Quenching cross sections for the $^3P$ state (open squares) and the $^4P$ state (filled circles), compared with the normalized geometric cross sections of the target outer-electron orbits (GEO) and electron capture cross sections predicted by semiempirical scaling rules[1,2] (EMP).

outer electron-shell divided by four. Overall, the quenching cross sections were in fair agreement with outer-shell electron capture cross sections predicted by semiempirical scaling rules, and those for Ne and Ar were very close to electron capture cross sections estimated from recent measurements of recoil ion production by 1.0 MeV/amu Ar ions. It is concluded, therefore, that direct capture to $Mg^{10+}$ ions from the outer-shells of the target gases is the principal mechanism for quenching x-ray emission from the $2^3P$ state.

Calculations employing the Oppenheimer-Brinkmann-Kramer model[3] indicate that the most probable $Mg^{10+}$ levels into which electrons are captured from the outer-orbitals of the noble gas targets studied are those for n = 2 and 3. The states that are produced have much shorter lifetimes than the original $^3P$ state since many radiative and Auger

branches are available,[4] and undoubtedly some fraction of them contribute to the spectator-electron transitions which underlie the $^3P$ peak.

The variation of the relative intensities of the prompt $KL^5$ and $KL^6$ peaks with increasing noble gas atomic number indicated that the average projectile charge resulting from a K-shell ionizing collision steadily decreased until it reached a minimum at Kr and then increased in going on to Xe.

References

1. A. S. Schlachter, J. W. Stearns, W. G. Graham, K. H. Berkner, R. V. Pyle and J. A. Tanis, Phys. Rev. A27, 3372 (1983).

2. A. S. Schlachter, K. H. Berkner, J. W. Stearns, W. G. Graham, E. M. Bernstein, M. W. Clark, J. A. Tanis, H. Schmidt-Bocking, S. Kelbch, J. Ullrich, S. Hagmann, P. Richard and M. P. Stockli, Nucl. Instrum. Methods B 24/25, 219 (1987).

3. V. S. Nikolaev, Zh. Eksp. Teor. Fiz. 51, 1263 (1966) [Sov. Phys. - JETP 24, 847 (1967)].

4. M. H. Chen, At. Data and Nucl. Data Tables 34, 301 (1986).

G. Design and Construction of an Atomic Physics Beamline for the ECR Ion Source (B. B. Bandong, L. Yang, L. Heffner, D. A. Church, R. E. Tribble, and R. L. Watson)

A two-stage 14.6/6.4 GHz) electron-cyclotron-resonance (ECR) ion source has been constructed recently for axial injection of intense beams of moderately to highly charged positive ions into the Texas A&M University K-500 Superconducting Cyclotron. Beam transport into the K-500 cyclotron is accomplished through the use of an axial injection line employing X-Y bending magnets, solenoid focusing lenses, and two $90^{o}$ bending magnets. Details of the ECR ion source configuration and the beam transport system are given elsewhere.[1] Table I shows the ion beams produced by the TAMU ECR ion source during initial test and beam development runs. Addition of metal vapor ovens to the ECR chamber would broaden the range of ions extractable from the source to include metallic ions such as Li, Na, Mg, Si, etc.

During periods when the cyclotron is not scheduled for experimental runs and beam development, the charge-analyzed beams from the ECR ion source can be transported into a new atomic physics beamline which is located on top of the cyclotron vault roof, alongside the ECR ion source. The concrete roof blocks provide sufficient radiation shielding to allow personnel to work around the source and the atomic physics facility even when the cyclotron is running. Since the source can be variably biased from -10 kV to +10 kV and the plasma chamber can be operated up to +30 kV, beam energies of 5 to 30 KeV/q (where q is the ion charge) can be obtained. Such beams are ideal for the study of

TABLE I. Ions produced by the TAMU ECR ion source during initial test runs. The extraction voltage was 10 kV. Also listed are the beam energies obtained from the K-500 cyclotron.

| Beam | Charge State q | eμA | Energy (MeV/amu) |
|---|---|---|---|
| $^{16}O$ | 7 | 8.0 | 40 |
| | 6 | 53.0 | 30 |
| | 5 | 59.0 | 30 |
| $^{40}Ar$ | 13 | 2.4 | 30 |
| | 12 | 8.3 | 30 |
| | 11 | 14.0 | 25 |
| | 9 | 27.0 | 20 |
| $^{84}Kr$ | 19 | 2.0 | 20 |
| | 17 | 3.6 | 15 |
| | 15 | 4.5 | 15 |

atomic processes in the low energy ion-atom collision regime. The high intensity beams will make possible experiments involving high resolution photon and electron spectroscopy, and will enable studies of state-selective electron capture processes.

The beam is switched from the cyclotron injection line into the atomic physics beamline by means of a third 90° bending magnet located approximately 4 meters from the first 90° analyzing magnet. The components of the atomic physics beamline are shown in Fig. 1. The vacuum system employs ConFlat type metal seals to allow bake-out of the entire line for better vacuum. One ion pump and two cryopumps are used to maintain a vacuum of $10^{-8}$ torr or better. Two sets of asymmetric quadrupole triplet electrostatic lenses provide for beam focusing. A beam steering box containing a four-jaw slit system, a Faraday cup, and

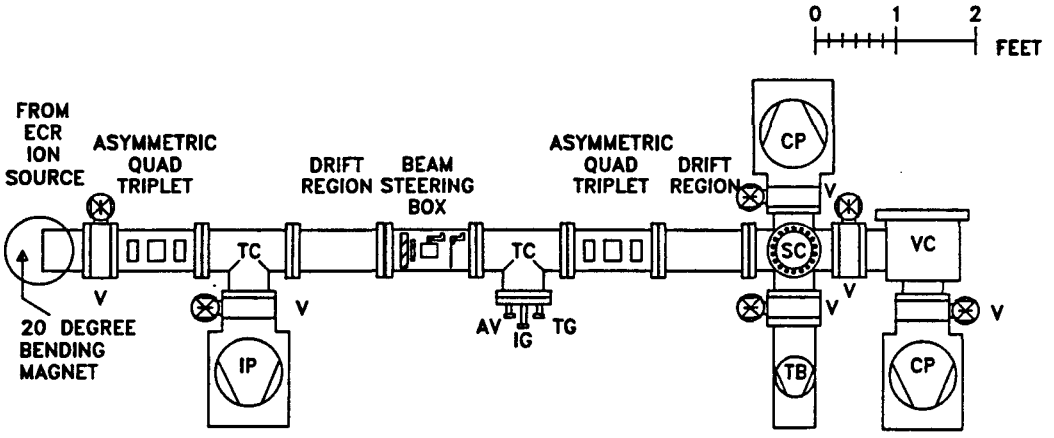


IP – 140 li/s ion pump
CP – 1000 li/s cryopump
TB – 360 li/s turbo-pump
SC – six-way cross
TC – "tee" connector
V – electropneumatic valve
IG – nude ionization gauge tube
TG – thermocouple gauge tube
AV – right-angle valve
VC – target vacuum chamber

Figure 1. Components of the atomic physics beamline.

a beam scanner (1 mm gauge Cu wire) provide beam diagnostics and collimation. Because fairly high fringe magnetic fields from the K-500 cyclotron are expected in the area near the ECR source, most of the beamline was constructed from sections of Ni-electroplated, low-carbon-steel pipe with wall thickness of 0.125 in. Other parts of the line, such as the electrostatic lenses and the slit box segments, are made from shielded stainless steel pipe segments.

The design and location of the quadrupole triplet lenses was based on first-order beam optics calculations performed to optimize the beam transport through the bending magnet and into the scattering chamber at the end of the atomic physics beamline. The computer code TRANSPORT[2] was used for these calculations with the electrostatic lenses simulated as magnet edges that focus in both planes. Fig. 2 shows the expected beam profile from the 90° bending magnet (at the beginning of the atomic physics beamline) to the scattering chamber. The figure shows the half-

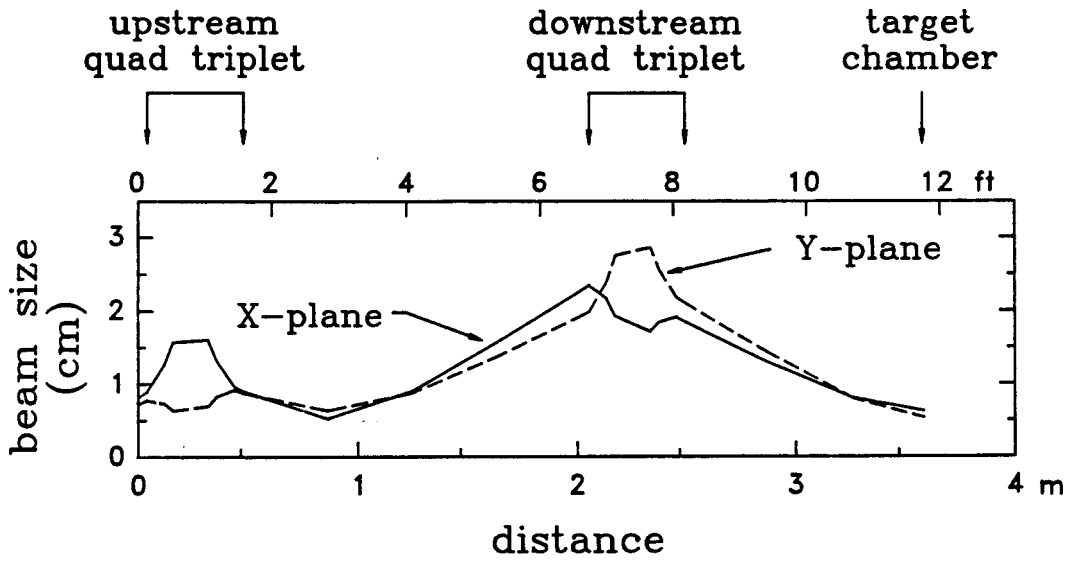


Figure 2. Calculated beam profile from the 90° bending magnet to the scattering chamber.

width of the beam in the X (horizontal) and Y (vertical) planes. The assumed emittance from the source is $10\pi$ cm-mrad in both X and Y planes. The calculations start at the first X-Y defining slit after the source, with a beam half-width equal to 0.5 cm in both planes. The 90° bending magnet on the atomic physics beamline is located just after a solenoid focusing lens which focuses the beam into a radial waist. Such a configuration allows the 90° magnet aperture requirement to be minimal, hence producing a lower-divergence beam that is easier to transport. The downstream quadrupole triplet lenses focus the beam on the target to a spot about 1 cm in diameter having a beam divergence of about 10 mrad.

The six-way cross (Huntington Model VF-6600) located in front of the scattering chamber provides additional experimental flexibility. Since it is fitted with a cryopump and pneumatic gate valves, it can serve as another target chamber. It will be used primarily for pre-

treatment of the ion beam via a charge-exchange gas cell or a laser prior to final impact on a target located in the scattering chamber.

The scattering chamber was designed to serve as a versatile, general purpose vacuum chamber and was constructed by Huntington Mechanical Laboratories. A sketch of the chamber is shown in Fig. 3. The dimensions (in inches) are also given in this figure. The radial ports on the chamber will accommodate experimental devices, analytical instruments, feedthroughs, and other accessories. A 3-3/8 in. O.D. size port is oriented directly downstream and will be fitted with a gate valve to allow connection of a supplemental target chamber. The top cover can be sealed by either a Cu wire or a Viton o-ring.

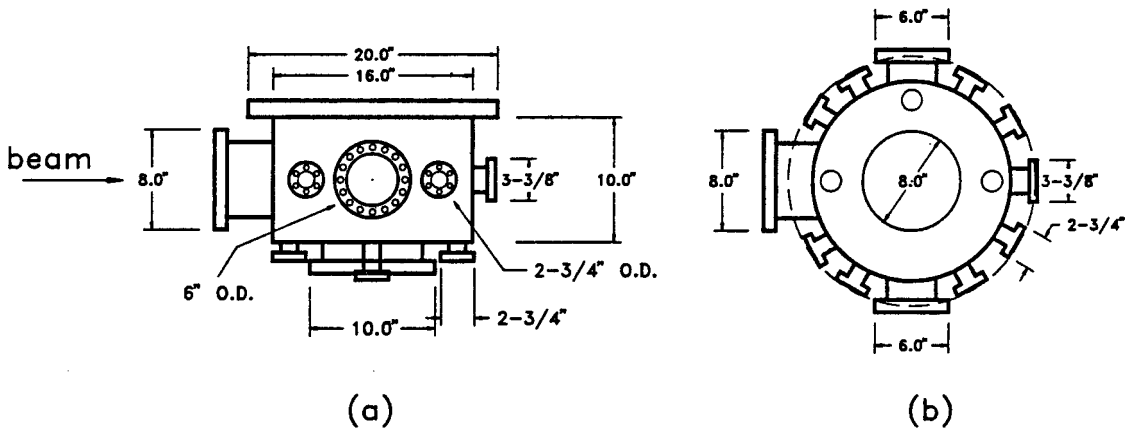


Figure 3. Scattering chamber on the atomic physics beamline.

**References**

1. D. P. May, R. C. Rogers, P. Smelser, G. Mouchaty, A. van Baalen, and P. Bowman, Proc. Intl. Conf. on ECR Ion Sources and their Applications, East Lansing, MI, ed. J. Parker, NSCL Rep. MSUCP-47, 364 (1987).

2. K. L. Brown and S. K. Howry, SLAC-91 UC-28, Stanford, CA (1970).

## V. APPENDIX

Reprints of publications for the grant period July 1, 1987 to January 1, 1990. reprints removed. ds.